BROADBAND MICROSTRIP LOOP ANTENNAS

By

JIANMING YANG

A Thesis
Submitted to the School of Graduate Studies
in Partial Fulfillment of the Requirements
for the Degree
Master of Engineering

McMaster University

MASTER OF ENGINEERING McMaster University

(Electrical Engineering) Hamilton, Ontario

TITLE : Resonant Microstrip Loop Antennas

AUTHOR : Jianming Yang

SUPERVISOR : Dr. John Litva

NUMBER OF PAGES : i - ix ; 1 - 75

Abstract

This thesis involves the development of a new and compact microstrip loop antenna which combines high gain and broad bandwidth in an easy to fabricate structure. The antenna has many potential applications as its geometrical layout makes it easy to design linear and planar arrays. Practical antennas in the form of 1-element, 2-element, 4-element and 8-element were successfully constructed and tested at the frequency band of 940-956 MHz for a personal communication service (PCS) system. Experimental investigations were also carried out for applications in the band of 2-GHz wireless telecommunication systems. Instead of the traditionally used uniform current approach, the antenna's radiation patterns are modeled in a more realistic fashion: a non-uniform current distribution approach. This approach yields formulas which can be conveniently used to predict the radiation patterns of the antenna and the antenna arrays. The theoretical component of the microstrip loop antenna is also presented in this thesis.

Acknowledgments

I would like to express my most sincere appreciation to my supervisor, Dr. John Litva, for providing me with the opportunity to work in a new area of engineering, that of microwave engineering. I would also like to thank him for the support, guidance, and encouragement he provided throughout the course of my graduate studies and research.

I feel fortunate to have been able to participate in a wide variety of interesting and exciting research programs at the Communications Research Laboratory (CRL) at McMaster University in the past few years. I would like to thank all of the staff working at CRL for making it a fun and pleasurable place to work. In particular, I must express my gratitude to Chen Wu for his guidance and assistance in this work.

Finally, I dedicate this thesis to my wife Haiyin and my daughter Julia.

Contents

List of Figures

List of Tables

Chapter 1

Introduction

1.1 Review of Microstrip Antennas

In the antenna field, microstrip antennas have played an increasingly active role since the mid-1970's, contributing new developments and applications. The most important feature of microstrip antennas is that the radiating element is made on a substrate board by using modern printed-circuit technique. This technique provides the microstrip antennas with significant advantages over conventional antenna designs, which are listed in the following[1][2][3]:

1. They are low profile, reduced weight and inexpensive to manufacture in large quantity.

2. They are easily conformable to nonplanar surfaces and are mechanically robust when attached to a rigid surface.

3. They are versatile elements and can be designed to produce a wide variety of patterns and polarization.

4. Adaptive elements can be made by simply adding appropriately placed pin or varactor diodes between the patch and the ground plane. Using such loaded elements one can vary the antenna's resonant frequency[4][5], polarization[4][6], impedance[7], and even the pattern by changing bias voltages on the diodes[8].

5. Applications can be expanded by grouping many identical radiating elements to build linear or planar arrays[9][10][11].

As the wireless telecommunication industry grows, there is an increasing demand for low profile, low cost and high performance microstrip antennas. It is reasonable to believe that research in the field will remain very active and is likely to continue for many years.

The microstrip antenna concept and its possible applications was first suggested by Deschamps in 1953 [12]. A long time after the original suggestion was made, the first actual microstrip antenna was built by Munson in 1973 [13]. His work was to develop a flat antenna which could be mounted on rockets or missiles, and this work is considered to have led to the birth of the new microstrip antenna industry. In 1979, a specialists' meeting was held in Las

Cruces, New Mexico. This meeting marked the beginning of an international interest in microstrip antennas [14].

A typical microstrip antenna is a rectangular patch antenna. The radiating element is printed on the top surface of a substrate board, and the ground plane is printed on the bottom surface. The substrate is very thin (the thickness dimension is in the range of 0.003 to 0.005 free-space wavelength), consequently the antenna bandwidth is very narrow and its radiation efficiency is very low. The typical values of the rectangular patch are 3-5 percent of bandwidth and 5-6 dB of gain.

Mathematical analysis of the microstrip antenna is initially carried out by using the transmission line model to represent the rectangular patches [15][16]. This method gives the simplest way to explain the physical mechanisms of the microstrip antenna. Another method is the cavity theory which gives deeper insight into the operation of microstrip antennas. This method is also called the modal-expansion cavity technique and can be used to analyze a number of geometrical shapes of the patches such as rectangular, circular disk, circular ring, semicircular, and triangular [17]. These two techniques were developed under a general assumption: the substrate is electrically thin, therefore, these techniques are not valid when the substrate becomes thick.

1.2 Tendencies of Current Research in the Areas Related to this Study

In recent research of microstrip antennas, broadbanding techniques and simulation algorithms are two of the particular interest areas that attract people's attention.

Broadbanding techniques: There have been numerous designs over the past two decades to improve the narrow operational bandwidth of typical microstrip patch antennas. Among those new designs, the strip-slot-foam-inverted patch antenna (SSFIP) attracts the most attention. Compared to the rectangular patch antenna, the SSFIP antenna is a stacked multilayer structure and has a increased spacing between the layers of radiating element and ground plane. With the stratified structure design, this antenna offers following desirable features:

1. The bandwidth can be significantly improved by this technique. For a single SSFIP radiating element antenna, the bandwidth achieves 13.2%, and the gain is measured between 8.2 to 8.8 dBi [18]. By putting an additional radiating element and another foam layer on the top of the single element antenna, a stacked SSFIP structure is formed, and the largest bandwidth reported is further increased to 33% [19].

2. Microstrip feedline and slot coupling techniques are used in the antenna design. There is no direct contact between the feed lines and the

radiators (no soldering), so it is easier to group many of the radiators to build antenna arrays.

3. Cross polarization or circular polarization antennas can be constructed by using a cross-slot and suitably weighted feedlines [20][21].

However, because of the increased thickness and multilayer structure, traditional simulation methods such as the transmission line model and the modal-expansion cavity technique are not valid for the case of the SSFIP antenna.

Simulation algorithms: Although microstrip antennas look relatively simple, the determination of the electromagnetic fields by solving Maxwell's equations or derived wave equations for the performance of microstrip structures is quite complicated. Microstrip antennas are usually made of two or more different media. Each individual medium is homogeneous but the combination of all layers forms an inhomogeneous structure. This leads to a highly complex problem that can only be solved with advanced computer techniques.

The finite difference time domain solution of Maxwell's equations (FDTD) and the moment method (MM) are two examples of numerical techniques whose applications in electrical engineering have developed rapidly in recent years [22][23][39]. It has been demonstrated that they are powerful and versatile techniques for more accurate analysis of electromagnetic phenomena. Many configurations of multilayer microstrip antennas have been successfully simulated using these techniques. However, these highly accurate simulations come at the expense of increased computer processing time. Problems arise when simulations are performed for larger structures such as antenna arrays, especially for structures with complicated shapes, curved boundaries, and fine details.

1.3 Contributions of the Research

Applications of the microstrip antenna have rapidly expanded in recent years. The antenna configurations have become more and more complicated in order to satisfy certain required characteristics such as wide bandwidth, low sidelobes, dual operation frequencies, multiple beams, dual polarization or circular polarization. Because of their complexity, most of these antennas have been designed experimentally until now. In order to develop a microstrip antenna for a given application, it is crucial to first have a good understanding of the physical mechanisms that governs the behavior of the antenna.

This study involves the development of a new microstrip loop antenna which has improved performance in terms of frequency bandwidth. In this new antenna, microstrip line feeding and electromagnetic coupling are combined in a compact radiator structure [24]. Investigations for single element, 2-element, 4-element, and 8-element arrays have been carried out in the frequency bands of a personal communication system (PCS/960 MHz) and a wireless telecommunication system (2 GHz), respectively [25]. Compared with the SSFIP technique, this antenna offers better performance, even though it uses a structure which is less complex than that of conventional microstrip antennas. It also follows that the antenna assembly is simpler.

The analysis of electrically large loops is frequently under the assumption of uniform current amplitude and phase [26][29]. However, in real situations the current does not behave this way. Based on a nonuniform electric current distribution, a radiation model for a resonant circular loop is also developed. This model results in the very simple formulas for the far fields radiated by the loop. These formulas can be easily used to predict the radiated field patterns for the microstrip loop antenna, as well as loop array antennas. They can also be used to determine the best spacing between array elements in a process of optimum design. Simulation results for the previous mentioned antennas are very close in comparison with experiment measurements.

Radiation modeling of the microstrip loop antenna is presented in chapter 3. Design considerations, experiment measurements and antenna simulation results are discussed in chapter 4.

Chapter 2

The Fundamentals of Microstrip Loop Antennas

In this chapter we give a review of definitions, theoretical concepts and mathematical formulations that will be used in the development of the microstrip loop antennas in this thesis. These can all be found in standard antenna reference books. They are presented here for the convenience of the reader.

In section 2.1 is given the formulations that can be used for calculating the fields radiated by a given antenna current distribution. A more detailed discussions is given by Stutzman and Thiele in [26]. Section 2.2 gives a brief discussion of thin-wire loop antennas. In sections 2.3 and 2.4 are given discussions on how one determines the current distribution for a circular loop antenna. Detailed discussions, which serves as the basis for the review given in this chapter, with regards to the theory underlying circular loop antennas, are given by King and Smith [28], Kraus [29], and Forster [30]. Section 2.5 gives a brief review of antenna array factors, which are discussed in detail by Wolff [35].

As a further development to existing methods for simulating circular loops, a practical radiation model for a resonant microstrip loop antenna is developed in Chapter 3.

2.1 Solution of Maxwell's Equations for Antenna Radiation

We shall consider here the electromagnetic fields **E** and **H** and the source charge density ϱ and the source current density **J** varying sinusoidally with time which is defined by the angular frequency ω. The electromagnetic equations are given in phasor-vector notation by:

$$
\begin{aligned}
&\nabla \times \mathbf{E} = -j\omega\mu\mathbf{H} \\
&\nabla \times \mathbf{H} = j\omega\varepsilon'\mathbf{E} + \mathbf{J} \\
&\nabla \cdot \mathbf{E} = \frac{\varrho}{\varepsilon'} \qquad (2.1) \\
&\nabla \cdot \mathbf{H} = 0 \\
&\nabla \cdot \mathbf{J} = -j\omega\varrho
\end{aligned}
$$

where $\varepsilon' = \varepsilon - j(\sigma/\omega)$.

The first four of these differential equations are referred to as the time-harmonic form of Maxwell's equations, and the last one as the continuity equation. The notations **E**, **H**, ϱ and **J** are complex-valued functions of spatial coordinates only. From the time derivative of the electromagnetic fields, the factor $j\omega$ is obtained and this factor indicates the time-varying property of the fields. The isotropic homogeneous medium is characterized by three constitutive parameters:

permittivity ε, permeability μ and conductivity σ. They are complex in general, but in many antenna problems they can be approximated as real quantities.

The antenna problem consists of solving Maxwell's equations for the far-fields E and H which are created by an impressed current distribution J on antennas. How one goes about deriving the current distribution depends on what kind of antenna one is dealing with. For microstrip antennas, it is not an easy task to determine the current J, because multilayer dielectric substrates are involved and Maxwell's equations are not as simple as expressed in equation (2.1) anymore. However, for the moment we suppose that the J is a known current distribution. With this assumption the antenna's radiation problem can be solved in a very straightforward way [26].

For obtaining the far-fields E and H, two potentials are introduced: the magnetic vector potential A and the electric scalar potential ϕ, and they are defined by:

$$\begin{aligned} \mathbf{H} &= \frac{1}{\mu}\nabla \times \mathbf{A} \\ \mathbf{E} + j\omega\mathbf{A} &= -\nabla\phi \end{aligned} \tag{2.2}$$

With this definition and the Lorentz Gauge : $\nabla \cdot \mathbf{A} = -j\omega\mu\varepsilon'\Phi$, the fields within equation (2.1) can be replaced by an expression in terms of the vector potential A:

$$\nabla^2 \mathbf{A} + \omega^2 \mu \varepsilon' \mathbf{A} = -\mu \mathbf{J} \tag{2.3}$$

This equation is called the vector wave equation, and the solution of this equation is given by:

$$\mathbf{A} = \iiint_V \mathbf{J} \frac{\mu e^{-j\beta R}}{4\pi R} dv$$

$$\beta = \omega\sqrt{\mu\varepsilon'} \tag{2.4}$$

where R is the distance vector measured from the source point to the observation point. For the antenna radiation problem in the far-field region, we usually assume that σ=0, so that ε'=ε. Then we have the above expression for β which is recognized as the phase constant for a plane wave

With the concept of vector potential A, we can summarize the procedure of finding the fields generated by a given current distribution J: first we solve the integral equation (2.4) and find the vector potential A, then we can obtain the far-fields H and E using the following formulas:

$$\mathbf{H} = \frac{1}{\mu} \nabla \times \mathbf{A}$$

$$\mathbf{E} = \frac{1}{j\omega\varepsilon} (\nabla \times \mathbf{H} - \mathbf{J}) \qquad \text{(in the source region)} \tag{2.5}$$

$$\mathbf{E} = \frac{1}{j\omega\varepsilon} \nabla \times \mathbf{H} \qquad \text{(in the field region)}$$

Antenna radiation patterns are defined as the graphical representations of the far-field intensity radiated by an antenna. In general the patterns are 3-dimesional surfaces. In most practical situations, the far-field patterns are presented in terms of the E-plane pattern and the H-plane pattern. E-plane and H-plane patterns are also referred to as the principal plane patterns, and they are 2-dimensional plots. The E-plane pattern is defined as the radiation pattern that is measured in the plane containing the electric vector, and the H-plane pattern is measured in the plane containing the magnetic field vector.

2.2 The Loop Antennas

The loop antenna is one of the most commonly used types of wire antennas. The applications of loop antennas date back to the early experiments of Hertz on electromagnetic wave propagation [27], and the earliest radio communication experiment was carried out using loop antennas on submarine boats [28].

Loop antennas are typically divided into small loops and larger loops according to electrical size. A loop whose dimension is less than about a tenth of a wavelength is called an electrically small loop antenna. Small loops are commonly used as receiving antennas. They are characterized by having a radiation pattern which is independent of the antenna shape and frequency.

Electrically larger loops, particularly those near resonant size, are used mainly as elements in directional arrays. It has been showed by Kraus that the far-field patterns of a square loop and a circular loop are identical for the electrically small case, but the patterns are different for the case of the larger loops (for example, when the loop dimension is increased to about 4~5λ) [29].

The radiation properties of thin-wire loop antennas are discussed in different ways. A simplified circular loop model was given by Foster [30]. In this model, the electric current on the loop is assumed to have uniform amplitude and in-phase. This approach gives a straightforward explanation for the physical mechanisms underlying the operation of loop antennas, and gives a simple formula to calculate the far-field patterns. However, the formula does not work well for the case of large loops, because when the loop size is increased close to a half-wavelength or larger, obviously the current is no longer uniformly distributed.

Stutzman and Thiele dealt with the problem of loop antennas from the view point of square loops. In their discussions, a uniform current distribution is used for the case of small loops, while a nonuniform current is employed for large loops [26].

The Fourier series analysis for the circular loop antenna is a relatively more comprehensive method. This method has a long history dating back to the work of H. C. Pocklington in 1897, in which he dealt with the analysis of the closed loop [28]. Recent treatments and detail discussions are given by R. W. P. King, Prasad [31] and F. J. Zucker [32]. As a result of the Fourier series analysis for circular loops, formulas are obtained, which can be used to calculate the loop antenna properties such as current distribution on loops, radiation patterns in far-field region, as well as antenna's input impedance and radiation impedance. These formulas are applicable to both electrically small and large circular loop antennas. Of the possible shapes for a loop antenna, the circular loop has received the most attention. One of the major reasons for its popularity is that the antenna properties of circular loops may be calculated using a closed form solution. However, the derivations used in this method look somewhat complicated. The formulas are not convenient for practical use, since they are composed of terms of the Fourier series. To ensure accurate results, a sufficiently large number of terms of the series have to be carried in the analysis (usually 20 terms). Special attention should also be paid while one carries out the calculation, because a number of intermediate variables are introduced in those formulas and their expressions are not in simple forms.

Our study purpose is to develop an model which can be easily used in practical antenna design. Therefore, in next section we will only present the related part of the loop antenna theory with Fourier series analysis: the electrical current distribution on a circular loop antenna. More detailed discussions about the rest parts of the theory are available in references [28], [31], and [33].

2.3 Electric Current Distribution on the Circular Loop Antenna [28-33, 35]

To determine the electric current distributed on the loop, the integral equation method is used. This integral equation is obtained from the boundary condition that requires the tangential component of the electric field to vanish at the conducting loop surface. Then, the electric field is determined by $\mathbf{E} = -\nabla\phi - j\omega\mathbf{A}$. The loop considered here is a very thin wire conductor. In other words, the radius of the wire a, is much smaller than the loop radius b. Thus, the field E in the above equation can be written in terms of its φ-component E_φ:

$$E_\varphi = \frac{-V_0\delta(\varphi)}{b} = -\left(\frac{1}{b}\frac{\partial\phi}{\partial\varphi} + j\omega A_\varphi\right) \tag{2.6}$$

where the term $V_o\delta(\varphi)$ represents a delta generator placed at a point $\varphi=0$, and it is defined as: $\int_{-\pi}^{\pi} bE_\varphi d\varphi = V_o$. The scalar potential ϕ and vector potential A on the loop surface at φ are given by:

$$\begin{aligned} \phi &= \frac{1}{4\pi\varepsilon}\int_{-\pi}^{\pi} q(\varphi')W(\varphi-\varphi')d\varphi' \\ A_\varphi &= \frac{\mu}{4\pi}\int_{-\pi}^{\pi} I(\varphi')W(\varphi-\varphi')\cos(\varphi-\varphi')d\varphi' \end{aligned} \tag{2.7}$$

In these two equations, ϕ is generated by the electric charge distributed on the surface of the loop, A is generated by the current in the loop wire, the notations φ and φ' are related to the observation point and the source point, respectively, and $W(\varphi-\varphi')$ is the kernel:

$$W(\varphi-\varphi') = \frac{b}{2\pi}\int_{-\pi}^{\pi}\frac{e^{-j\beta r}}{r}d\psi$$

$$r \approx \sqrt{4b^2\sin^2\frac{\varphi-\varphi'}{2}+B^2} \tag{2.8}$$

$$B \approx 2a\sin\frac{\psi}{2}$$

The definitions of φ, φ', r, B, and ψ are shown in Fig. 2.1 [31]. In the equation of continuity (in previous section 2.1) $\nabla\times J=-j\omega\varrho$, the φ-dimensional distributed charge $q(\varphi')$ and the current $I(\varphi')$ are related as:

$$\frac{1}{b}\frac{dI(\varphi')}{d\varphi'} + j\omega q(\varphi') = 0 \tag{2.9}$$

Now substitute (2.9) into (2.7) and then take the derivative, it follows that

$$\frac{\partial\phi}{\partial\varphi} = -\frac{-j}{4\pi\varepsilon\omega b}\int_{-\pi}^{\pi}\frac{\partial I(\varphi')}{\partial\varphi'}\frac{\partial}{\partial\varphi'}W(\varphi-\varphi')d\varphi' \tag{2.10}$$

After an integration by parts, it becomes

$$\frac{\partial\phi}{\partial\varphi} = \frac{j}{4\pi\varepsilon\omega b}\frac{\partial^2}{\partial\varphi^2}\int_{-\pi}^{\pi}I(\varphi')W(\varphi-\varphi')d\varphi' \tag{2.11}$$

By combining equations (2.11), (2.7) and (2.6), an integral equation for the distribution of current is obtained:

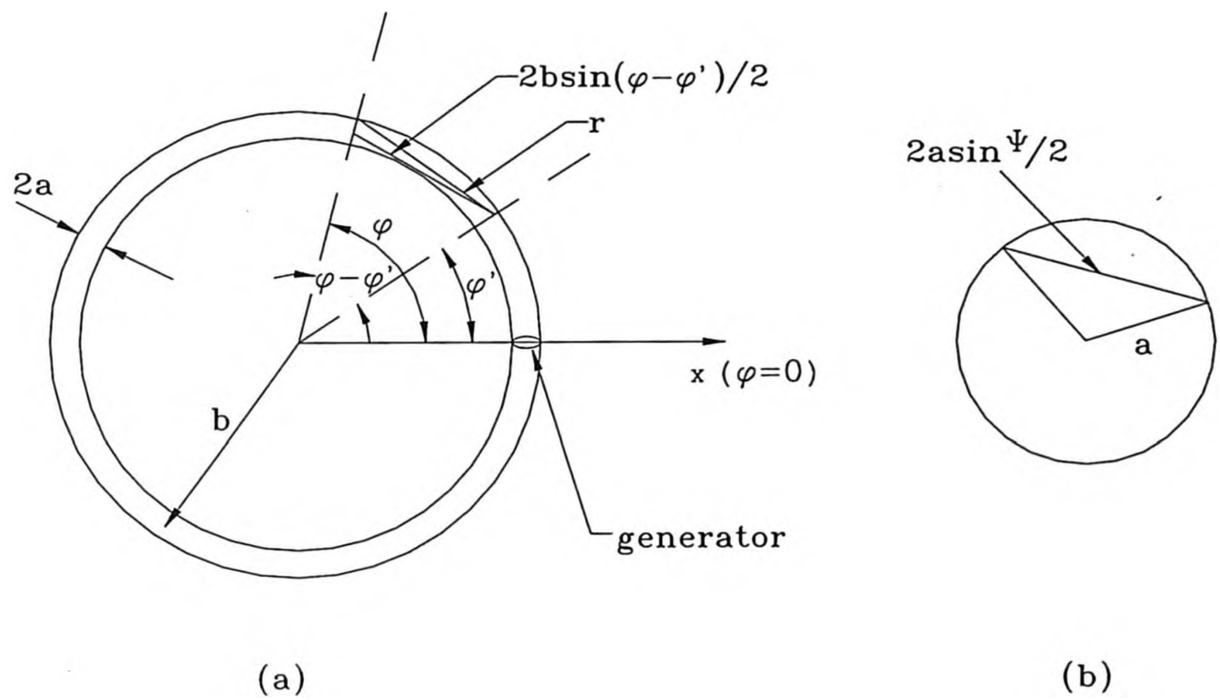

Fig. 2.1 *(a) Circular Loop and the notations, used in (2.8) on page 16*

r: distance from source point to observation point

φ': source point location in angular coordinate

φ: observation point location in angular coordinate

a: radius of the thin wire

b: radius of the circular loop

(b) The cross section of the wire and the notations, (B and ψ) used in (2.8) on page 16

$$V_o\delta(\theta) = \frac{j\zeta}{4\pi}\int_{-\pi}^{\pi} K(\varphi-\varphi')I(\varphi')d\varphi'$$

$$K(\varphi-\varphi') = \left[\beta b\cos(\varphi-\varphi') + \frac{1}{\beta b}\frac{\partial^2}{\partial\varphi^2}\right]W(\varphi-\varphi') \qquad (2.12)$$

$$\zeta = \frac{\omega\mu}{\beta} = \sqrt{\frac{\mu}{\varepsilon}}$$

With the aid of Fourier series expansions on the interval $-\pi \le \varphi \le \pi$, the $W(\varphi-\varphi')$ and $K(\varphi-\varphi')$ may be expressed as:

$$W(\varphi-\varphi') = \sum_{n=-\infty}^{\infty} K_n e^{-jn(\varphi-\varphi')}$$

$$K(\varphi-\varphi') = \sum_{n=-\infty}^{\infty} a_n e^{-jn(\varphi-\varphi')} \qquad (2.13)$$

where the coefficient K_n and a_n are given by:

$$K_n = K_{-n} = \frac{1}{2\pi}\int_{-\pi}^{\pi} W(\varphi-\varphi')e^{jn(\varphi-\varphi')}d(\varphi-\varphi')$$

$$a_n = a_{-n} = \frac{\beta b}{2}\left(K_{n+1} + K_{n-1}\right) - \frac{n^2}{\beta b}K_n \qquad (2.14)$$

We may also expand the current $I(\varphi)$ in a Fourier series form:

$$I(\varphi) = \sum_{n=-\infty}^{\infty} I_n e^{-jn\varphi}$$

$$I_n = \frac{1}{2\pi}\int_{-\pi}^{\pi} I(\varphi')e^{jn\varphi'}d\varphi' \tag{2.15}$$

Substituting equations (2.13), (2.14) and (2.15) into (2.12), we can finally obtain the expression of the current in the circular loop:

$$I(\varphi) = \frac{-jV_o}{\zeta\pi}\left(\frac{1}{a_o} + 2\sum_{n=1}^{\infty}\frac{\cos n\varphi}{a_n}\right) \tag{2.16}$$

Equation (2.16) provides a useful tool for circular loop antenna analysis and design. This formula can be used to calculate the current distribution in a loop of arbitrary electrical size. Once the current is obtained, the antenna's properties such as radiation patterns, input impedance, and radiation resistance can be further determined.

As can be seen in equation (2.16), the formula has a constant term and an infinite number of Fourier series terms. It has been proved that the theoretical calculation obtained by using 20 terms in the series corresponds well with measured values[33].

For electrically small loops, the dominant term in equation (2.16) is the constant term. This means that the current is uniformly distributed in the small loops. For the loop size near that of resonant conditions (the loop circumference $2\pi b=1\lambda$, 2λ, ..., for instance), the dominant term in Fourier series is the one where n is the corresponding integer. In particular, when the loop size is near the first resonance $2\pi b=1\lambda$, the loop is referred to as a resonant loop

2.4 Resonant Circular Loop Antenna

The resonant loop is the most frequently used electrically large loop because it has a reasonable input resistance, $R\approx100\ \Omega$ [33]. This feature is a favorite in practice for matching the antenna to a transmission line. The resonant frequency of a resonant loop can be easily determined by calculating the loop circumference:

$$2\pi b = \lambda_g \tag{2.17}$$

where b is the median radius of the loop, and λ_g is the wavelength in dielectric substrate. Correspondingly, the current distribution presented in equation (2.16) may be replaced by a simple form:

$$I(\phi) = I_0 \cos\phi \qquad 0 \leq \phi \leq 2\pi \tag{2.18}$$

where I_0 is the current amplitude coefficient. Fig. 2.2 is the plot of the current that is symmetrically distributed about the y-axis. The current maxima points are at the generator ($\phi=0$) and at the diametrically opposite point ($\phi=\pi$). The electrical current nodes are located at $\phi=\pi/2$ and $3\pi/2$.

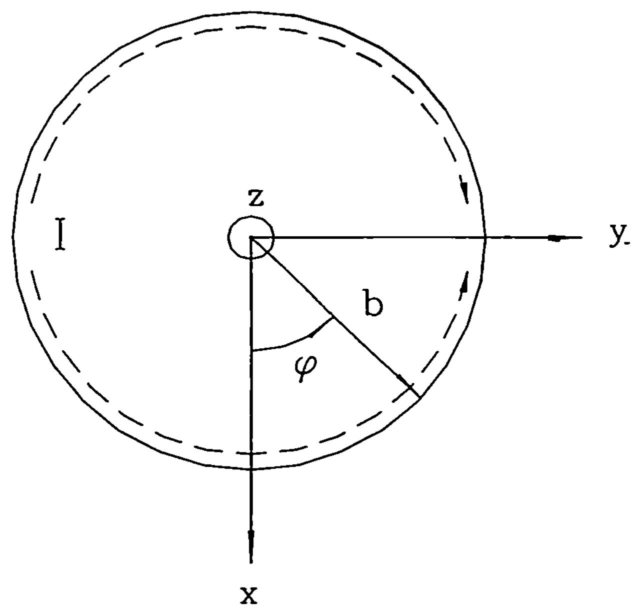

Fig. 2.2 *The Current Distribution in the Resonant Circular Loop*

2.5 Linear and Planar Array Factors

An antenna array is defined to consist of a group of individual radiators distributed in a linear or two-dimensional spatial configuration. By controlling the amplitude and phase excitation of each radiator, we can obtain a radiated beam of any desired shape in space. In communication systems, antennas array can be used to direct high-gain beams toward distant receivers and transmitters. The radiation pattern of the array is determined by the type of individual elements used, their orientation, their positions in space, and the amplitude and phase of the currents feeding them.

In this section, we shall briefly review the discussions on the basic forms of linear array and planar array[26][35], and present the array factors of each form. These two factors shall be used in the discussion of microstrip loop antenna's modeling in next chapter.

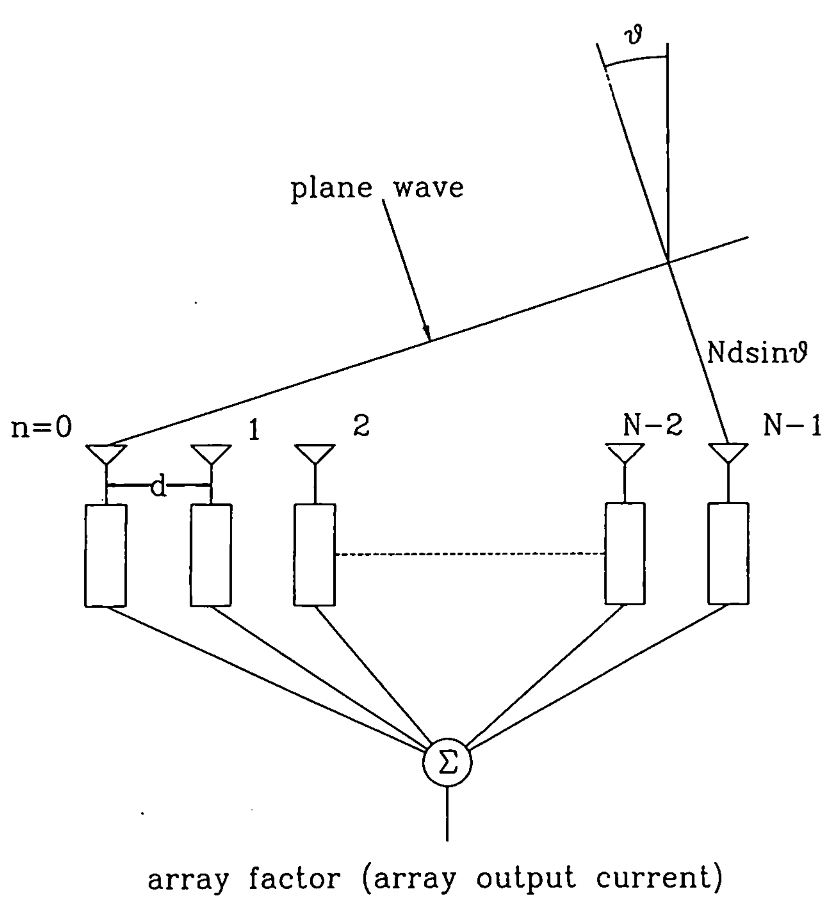

Fig. 2.3 *A basic linear array configuration*

Fig. 2.3 shows the basic configuration of the linear array, consisting of N radiators equally spaced at a distance d apart. This array works as a receiving antenna, but by reciprocity its receiving pattern is the same as the transmitting pattern. The signal from a distant transmitting antenna is represented in Fig. 2.3 by a plane wave with an incident angle of θ measured from the normal direction of the array. The current output of the array is referred to as array factor and is given in the following form:

$$\begin{aligned} AF &= A_o + A_1 e^{j\psi} + A_2 e^{j2\psi} + A_3 e^{j3\psi} + \cdots + A_{N-1} e^{j(N-1)\psi} \\ &= A_o \left[1 + e^{j\psi} + e^{j2\psi} + e^{j3\psi} + \cdots + e^{j(N-1)\psi}\right] \end{aligned} \tag{2.19}$$

where we have assumed that $A_o = A_1 = \cdots = A_{N-1}$.

Since

$$AF \times e^{j\psi} = A_o \left[e^{j\psi} + e^{j2\psi} + e^{j3\psi} + \cdots + e^{jN\psi}\right] \tag{2.20}$$

we have

$$AF - AFe^{j\psi} = AF\left(1 - e^{j\psi}\right) = A_o\left(1 - e^{jN\psi}\right) \tag{2.21}$$

or

$$AF = A_o \frac{\left(1 - e^{jN\psi}\right)}{\left(1 - e^{j\psi}\right)}$$

$$= A_o e^{j\left(\frac{N-1}{2}\right)\psi} \frac{\sin\left(\frac{N\psi}{2}\right)}{\sin\left(\frac{\psi}{2}\right)} \qquad (2.22)$$

where, $\psi=\beta_o d\sin\theta$ is the phase shift between the two adjacent elements. This expression has a maximum value at $\psi=0$ (in the direction of $\theta=0$):

$$AF(\psi = 0) = A_o N \qquad (2.23)$$

Dividing this value into equation (2.22), we obtain the normalized array factor $f(\psi)$:

$$f(\psi) = \frac{\sin\left(\frac{N\psi}{2}\right)}{N\sin\left(\frac{\psi}{2}\right)}$$

$$\psi = \beta_o d\sin\theta \qquad (2.24)$$

$$\beta_o = \frac{2\pi}{\lambda_o}$$

As an example of the pattern given by equation (2.24), Fig. 2.4 shows the array factor of a 10-element linear array, in which the elements are uniformly excited, and equally spaced with a distance of 0.5 wavelength.

In order to provide beam scanning in any direction in a 3-dimension space, a planar array of radiating elements must be used. The method for obtaining array factor in the case of linear array can be extended to planar array situation, resulting in the following expression:

$$AF = \left[\frac{\sin\left(\pi M \frac{d_x}{\lambda} \sin\theta \cos\phi \right)}{M \sin\left(\pi \frac{d_x}{\lambda} \sin\theta \cos\phi \right)} \right] \left[\frac{\sin\left(\pi N \frac{d_y}{\lambda} \sin\theta \sin\phi \right)}{N \sin\left(\pi \frac{d_y}{\lambda} \sin\theta \sin\phi \right)} \right] \tag{2.25}$$

Equation (2.25) is used for the uniformly excited rectangular array with M×N elements. The symbols d_x and d_y are the spaces between two adjacent elements in the x- and y-directions, respectively.

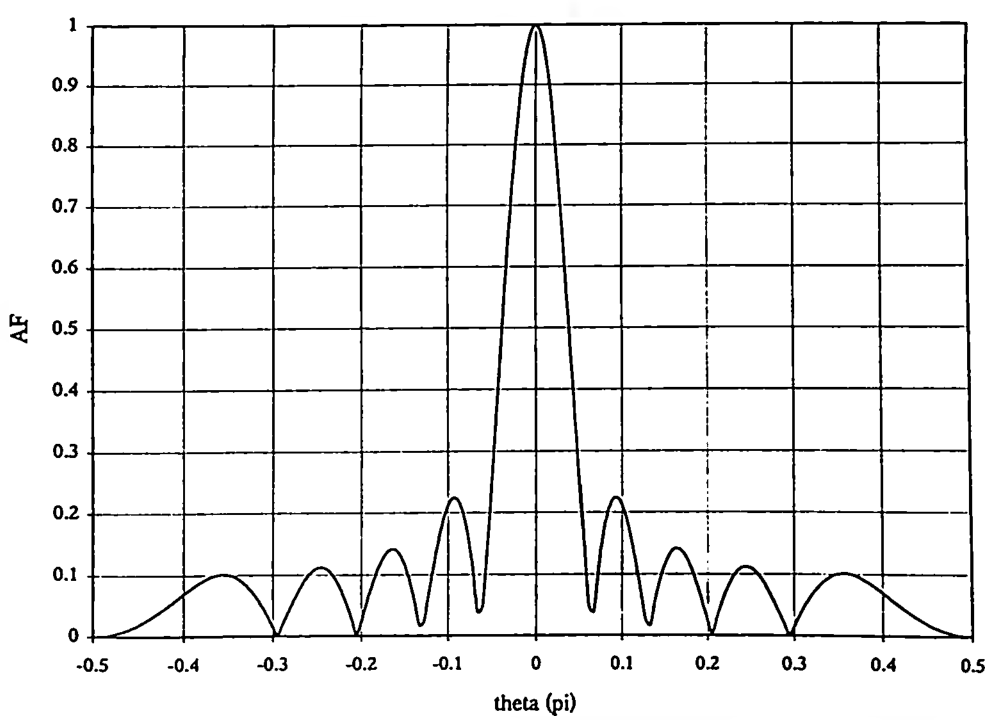

Fig 2.4 *Plot of array factor for a 10-element linear array*

Chapter 3

Radiation Model of the Microstrip Loop Antennas

In previous review of the existing analyses for circular loop antennas, we noted that the uniform current method is only suitable for modeling the electrically small loops, while the Fourier series method is not convenient for practical antenna design. This chapter introduces an alternative approach that gives the far-field expressions for the circular resonant loop antennas. The objective is to provide an antenna model which gives a clear physical insight and can be easily used to predict the radiation patterns not only for single element radiator, but also for linear and planar arrays. Since in most practical situations the antenna patterns are represented in terms of the E-plane pattern and the H-plane pattern, we will focus our attention on obtaining the far-field expressions in these two planes.

3.1 Equivalent Circular Loop of the Microstrip Loop Antenna

The microstrip loop antenna is shown in Fig. 3.1 (a), which consists of two dielectric substrate plates. The radiating element is a ring patch printed on the top surface of the first plate. The second plate is commonly referred to as the ground plane which is located at a certain distance from the first plate. More detail descriptions about the antenna configuration and design considerations will be given in the next chapter.

In order to simplify the modeling procedure, we assume that the microstrip loop antenna can be replaced by an equivalent thin-wire loop which is placed beyond an infinitely large perfect electric conductor plane as shown in Fig. 3.1 (b).

We may make this assumption mainly because what we are dealing with is a radiation problem in far field region. This can be further explained as:

1. the width of the microstrip ring patch is much smaller than the dimension of the ring's median circumference, so we may replace the patch with a thin circular wire having the same dimension of the circumference;

2. the thickness of antenna substrate is much smaller than the spacing between the radiating plate and the ground plate, so we may ignore the effect of the antenna substrate.

With this assumption, our original problem now becomes to determine the far field patterns radiated by the equivalent thin-wire circular loop.

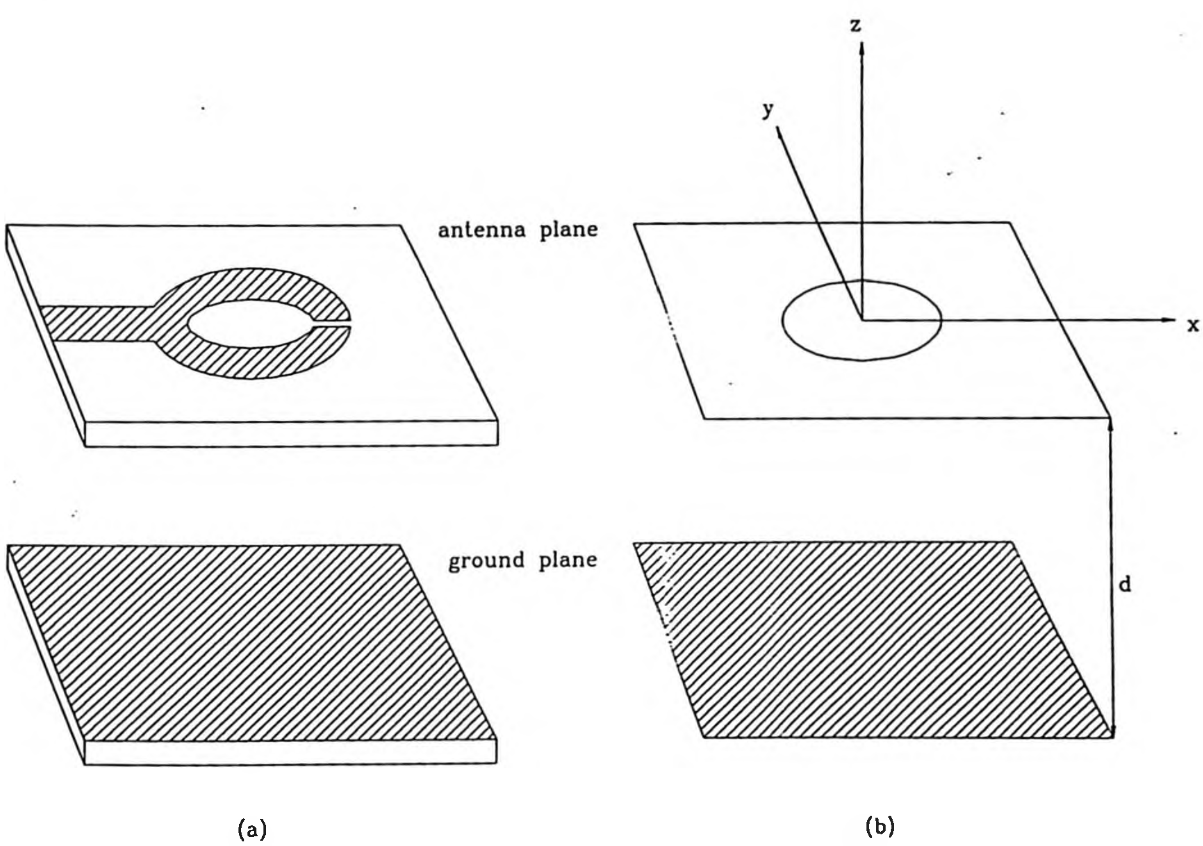

Fig. 3.1 *(a) Microstrip loop antenna,*

(b) Equivalent circular loop beyond a perfect conductor plane

Before we derive the radiation patterns, let us place the equivalent circular loop in the xy-coordinate plane with its center at the origin of the rectangular coordinates x, y, z and the spherical coordinates R_o, θ, Φ, as shown in Fig. 3.2. The loop is driven by a point-source generator of voltage V at the position Φ'=0.

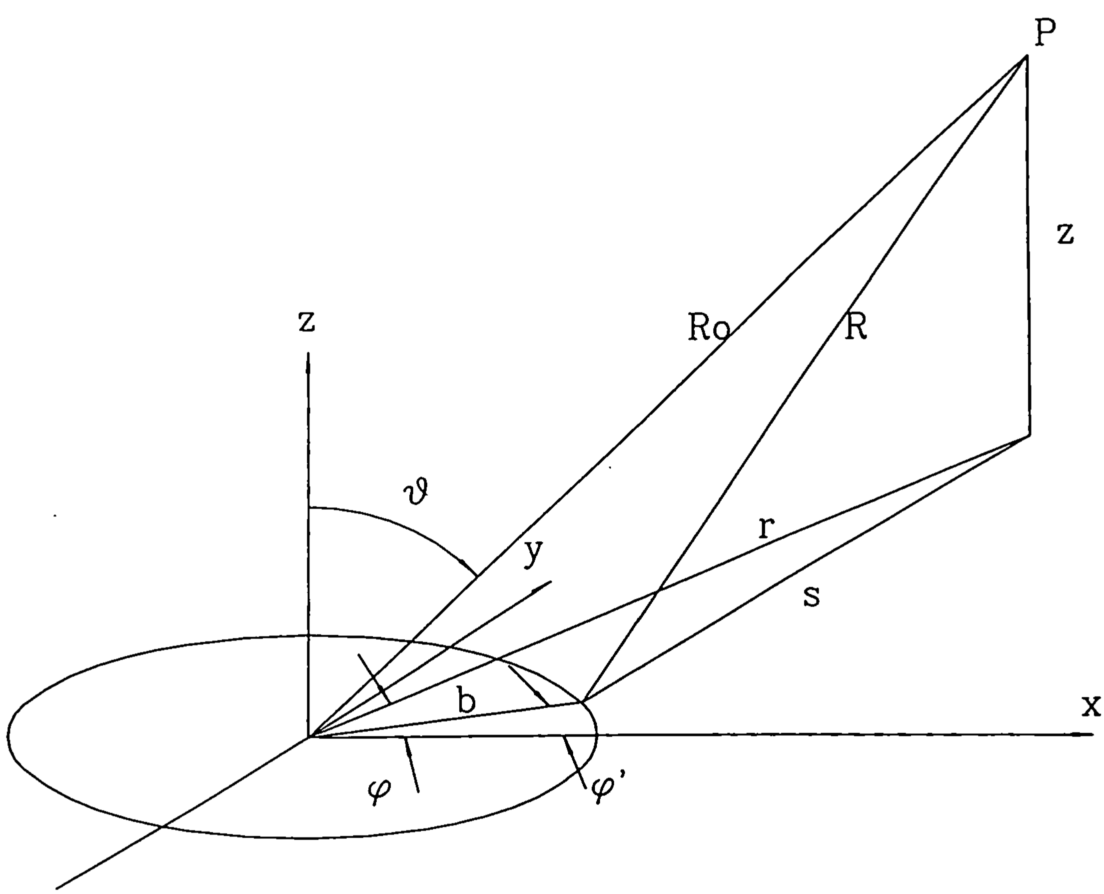

Fig. 3.2 Vector Potential dA at P-point due to the Current Element dI

Because the antenna is working at its first resonant frequency, the radius of the loop (b in Fig. 3.2) is given by equation (2.17), and the current distributed on the loop is given by equation (2.18). Then, we define the notations which are used in Fig. 3.2 and in the later discussions in sections 3.2 and 3.3. A source point is defined on the loop with a angular coordinate ϕ'. P is the observation point which is located in far-field region and defined by coordinates R_o, θ, and ϕ. The distance between the source point and the observation point is R. The notations r and s are the intermediate parameters, which are used only for convince of discussion. Clearly, they are determined by $s^2=r^2+b^2-2rb\cos(\phi-\phi')$, and $r=R_o\sin\theta$, respectively.

3.2 The Vector Potential A of the Resonant Loop Antenna

Now, let us consider an infinitesimal current element $I(\Phi')dl$ in the loop and a vector potential element dA generated by this current element. As illustrated in Fig. 3.3, the current element $I(\Phi')dl$ may be presented in terms of x and y directional components as:

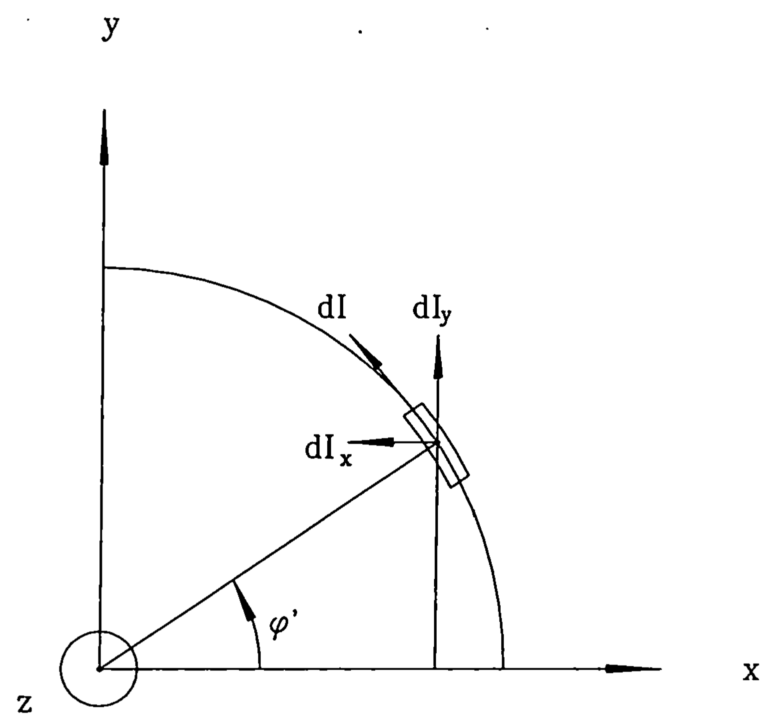

Fig. 3.3 *The Infinitesimal Current Element and the x- and y-components*

$$dI_x = -I(\phi')\sin\phi' dl$$
$$dI_y = I(\phi')\cos\phi' dl \qquad (3.1)$$

Correspondingly, the potential dA generated at the field point P(x, y, z) or P(R_o, θ, Φ) can be presented as:

$$dA_x = \frac{\mu}{4\pi}\frac{e^{-j\beta_o R}}{R}dI_x$$

$$dA_y = \frac{\mu}{4\pi}\frac{e^{-j\beta_o R}}{R}dI_y \qquad (3.2)$$

where β_o is the phase coefficient given by $\beta_o = 2\pi/\lambda_o$ (λ_o is the wavelength in free space), and R is the distance between the source point and the observation point P:

$$R^2 = z^2 + s^2 = R_o^2 \cos^2\theta + s^2 \qquad (3.3)$$

where R_o is measured from the origin to point P. Referring to the triangle having sides b, s, and r in Fig. 3.2, and using the cosines law, we have:

$$s^2 = R_o^2 \sin^2\theta + b^2 - 2bR_o \sin\theta\cos(\phi - \phi') \qquad (3.4)$$

It is assumed that the observation point is located sufficiently far distance from the loop, so that :

$$b^2 << R_o^2 \qquad (3.5)$$

The distance R is then approximated by:

$$R \approx R_0 - b\sin\theta\cos(\phi - \phi') \qquad (3.6)$$

Substituting equations (3.1) and (3.6) into (3.2), we have:

$$dA_x = \frac{-\mu}{4\pi}\frac{e^{-j\beta_o R_o}}{R_o} I(\phi')\sin\phi' dl\left[e^{j\beta_o b\sin\theta\cos(\phi-\phi')}\right]$$

$$dA_y = \frac{\mu}{4\pi}\frac{e^{-j\beta_o R_o}}{R_o} I(\phi')\cos\phi' dl\left[e^{j\beta_o b\sin\theta\cos(\phi-\phi')}\right] \tag{3.7}$$

Note that we may ignore the effect of $b\sin\theta\cos(\phi-\phi')$ on the amplitude but we may not ignore the effect on the phase when we substitute (3.6) into (3.2).

Equation (3.7) is the vector potential dA generated by only one source current element dI in the loop. To obtain the total vector potential A, we have to integrate all the contributions from every element in the loop.

As mentioned before, the resonant circular loop has a symmetrical current distribution. This feature can be used to simplify the integration procedure. Let us consider the two exciting sources: a pair of current elements diametrically opposed in the loop as shown in Fig. 3.4. Since these two elements are equal in amplitude but out of phase with each other, their contribution to the field point P can be written as:

$$dA_x = \frac{-\mu}{4\pi}\frac{e^{-j\beta_o R_o}}{R_o} I(\phi')\sin\phi' dl\left[e^{j\beta_o b\sin\theta\cos(\phi-\phi')} + e^{-j\beta_o b\sin\theta\cos(\phi-\phi')}\right]$$

$$dA_y = \frac{\mu}{4\pi}\frac{e^{-j\beta_o R_o}}{R_o} I(\phi')\cos\phi' dl\left[e^{j\beta_o b\sin\theta\cos(\phi-\phi')} + e^{-j\beta_o b\sin\theta\cos(\phi-\phi')}\right] \tag{3.8}$$

and the total A should be evaluated in the integral region of $-\pi/2 \le \Phi' \le \pi/2$:

$$A_x = \frac{-\mu}{2\pi}\frac{bI_o e^{-j\beta_o R_o}}{R_o}\int_{\frac{-\pi}{2}}^{\frac{\pi}{2}} \sin\phi'\cos\phi'\cos[\beta_o b\sin\theta\cos(\phi-\phi')]d\phi'$$

$$A_y = \frac{\mu}{2\pi}\frac{bI_o e^{-j\beta_o R_o}}{R_o}\int_{\frac{-\pi}{2}}^{\frac{\pi}{2}} \cos\phi'\cos\phi'\cos[\beta_o b\sin\theta\cos(\phi-\phi')]d\phi' \tag{3.9}$$

Equation (3.9) gives the vector potential A at an arbitrary far-field point P. Substituting equation (3.9) into previously discussed equation (2.5), the electromagnetic fields E and H at the same point can be obtained. In next section, we shall derive the field pattern expressions in the E-plane and H-plane, respectively.

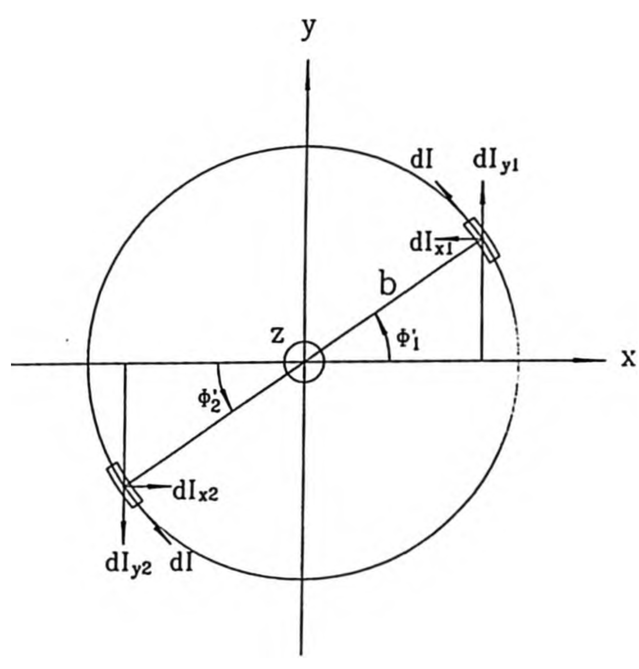

Fig. 3.4 *A Pair of Exciting Current Elements for the Case of Resonant Circular Loop*

3.3 Radiation Patterns in the E-plane and H-plane

3.3.1 The E-plane Pattern of the Circular Resonant Loop

According to the definitions of the E-plane and H-plane (section 2.1) and the current equation (2.18), we know that the E-plane is the yz-plane (or the plane: $\phi\equiv\pi/2$), and the H-plane is the xz-plane (or the plane: $\phi\equiv 0$). Let us first deal with the E-plane pattern.

Consider an arbitrary pair of infinitesimal current elements located symmetrically to the y-axis, as shown in Fig. 3.5. Since the x-components of current are equal in size but opposite in direction, only the y-components of current give contribution to radiation patterns in the E-plane.

Substituting $\phi=\pi/2$ and $\cos(\pi/2-\phi')=\sin\phi'$ into equation (3.9), we have:

$$A_{x_e} = 0$$

$$A_{y_e} = \frac{\mu}{2\pi}\frac{bI_o e^{-j\beta_o R_o}}{R_o}\int_{\frac{-\pi}{2}}^{\frac{\pi}{2}} \cos^2\phi' \cos\left[(\beta_o b \sin\theta \sin\phi')\right] d\phi' \tag{3.10}$$

By introducing the new variable Ψ:

$$\psi = \phi' + \frac{\pi}{2}$$

$$\cos\phi' = \sin\psi$$

$$\sin\phi' = -\cos\psi \tag{3.11}$$

$$\cos^2\phi' = \sin^2\psi = \frac{1}{2}(1-\cos 2\psi)$$

$$d\phi' = d\psi$$

we have:

$$A_{ye} = \frac{\mu}{2\pi}\frac{bI_o e^{-j\beta_o R_o}}{R_o}\int_{\frac{-\pi}{2}}^{\frac{\pi}{2}}\cos^2\phi'\cos[\beta_o b\sin\theta\sin(\phi')]d\phi'$$

$$= \frac{\mu}{2\pi}\frac{bI_o e^{-\beta_o R_o}}{R_o}\int_{\psi=0}^{\pi}\frac{1}{2}(1-\cos 2\psi)\cos[-\beta_o b\sin\theta\cos\psi]d\psi$$

$$= \frac{\mu}{4}\frac{bI_o e^{-j\beta_o R_o}}{R_o}\left[\frac{1}{\pi}\int_{\psi=0}^{\pi}\cos(u\cos\psi)d\psi - \frac{1}{\pi}\int_{\psi=0}^{\pi}\cos 2\psi\cos(u\cos\psi)d\psi\right] \tag{3.12}$$

$$= \frac{\mu bI_o e^{-j\beta_o R_o}}{4R_o}[J_o(u)+J_2(u)]$$

where $u=\beta_o b\sin\theta$, and $J_i(u)$ is the Bessel functions given by:

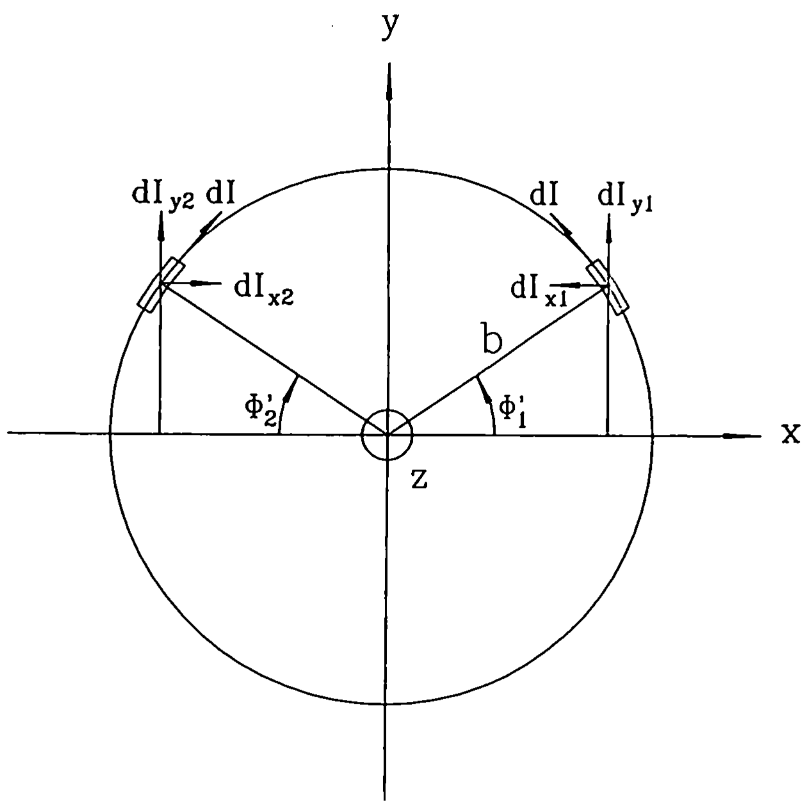

Fig. 3.5 *Only the y-components make contribution to the E-plane pattern*

$$J_0(u) = \frac{1}{\pi} \int_{\psi=0}^{\pi} \cos(u\cos\psi) d\psi$$

$$J_2(u) = -\frac{1}{\pi} \int_{\psi=0}^{\pi} \cos(u\cos\psi)\cos 2\psi d\psi \qquad (3.13)$$

$$\vdots$$

$$J_n(u) = \frac{1}{\pi} \int_{\psi=0}^{\pi} \cos(u\sin\psi)\cos n\psi d\psi$$

Than, we can rewrite the y-component of A (3.12) in the E-plane as :

$$A_{ye} = \frac{\mu b I_o e^{-j\beta_o R_o}}{4R_o}\left[J_0(\sin\theta) + J_2(\sin\theta)\right] \tag{3.14}$$

Finally, the radiation field intensity E in the far-field region can be obtained by substituting A (3.14) into E = -jωA (2.2) :

$$E_{ye} = \frac{-j\omega\mu b I_o e^{-j\beta_o R_o}}{4R_o}\left[J_0(\sin\theta) + J_2(\sin\theta)\right] \tag{3.15}$$

3.3.2 The H-plane Pattern of the Circular Resonant Loop

For the H-plane (xz-plane) patterns, we consider an arbitrary pair of current elements located symmetrically to the x-axis. Note that the x-components of the currents remain equal in size but out of phase with each other (Fig. 3.6), so the x-component still contributes nothing to antenna radiation in far-field region, and only y-component has to be taken into account.

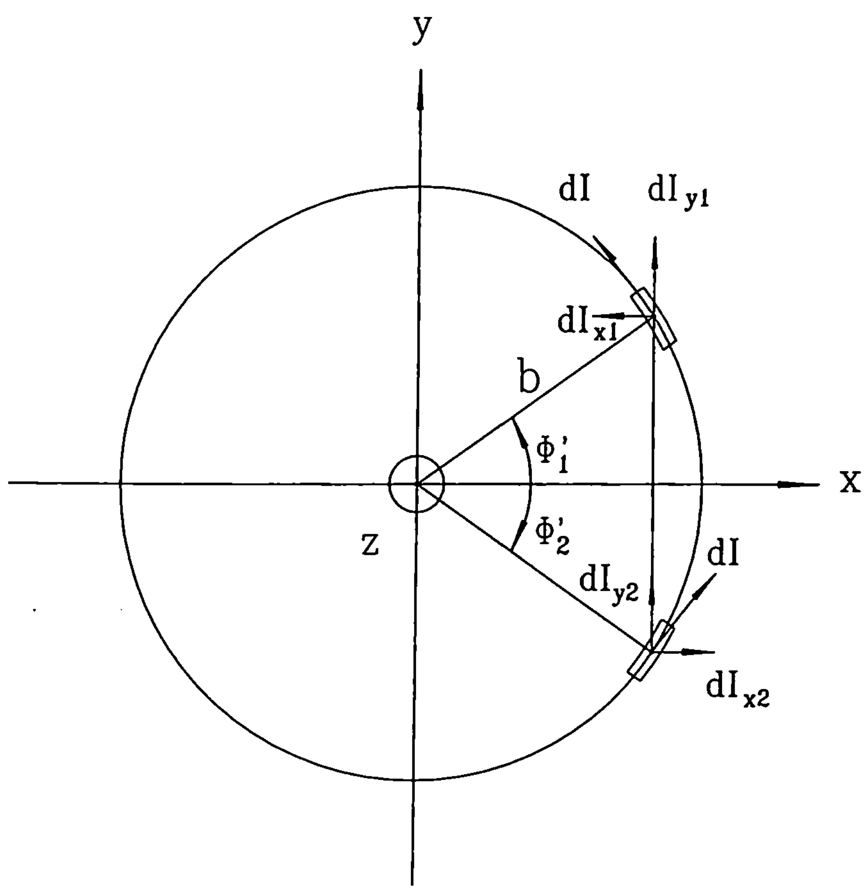

Fig. 3.6 *Only the y-components make contribution to the H-plane pattern*

Substituting the H-plane conditions $\phi=0$ and $\cos(0-\phi')=\cos\phi'$ into equation (3.9) gives:

$$A_{xh} = 0$$

$$A_{yh} = \frac{\mu}{2\pi}\frac{bI_o e^{-j\beta_o R_o}}{R_o}\int_{\frac{-\pi}{2}}^{\frac{\pi}{2}} \cos^2\phi' \cos\left[\beta_o b \sin\theta \cos(\phi')\right] d\phi' \tag{3.16}$$

Using the new variety Ψ and (3.11), we have:

$$A_{yh} = \frac{\mu}{2\pi}\frac{bI_o e^{-j\beta_o R_o}}{R_o}\int_{\frac{-\pi}{2}}^{\frac{\pi}{2}} \cos\phi' \cos\phi' \cos\left[\beta_o b \sin\theta \cos(\phi')\right] d\phi'$$

$$= \frac{\mu}{4}\frac{bI_o e^{-j\beta_o R_o}}{R_o}\left[\frac{1}{\pi}\int_{\psi=0}^{\pi} \cos(u\sin\psi) d\psi - \frac{1}{\pi}\int_{\psi=0}^{\pi}\cos 2\psi \cos(u\sin\psi) d\psi\right] \tag{3.17}$$

$$= \frac{\mu b I_o e^{-j\beta_o R_o}}{4R_o}\left[J_0(u) - J_2(u)\right]$$

where $u=\beta_o b\sin\theta$, and $J_i(u)$ is the Bessel functions and given by:

$$J_0(u) = \frac{1}{\pi}\int_{\psi=0}^{\pi} \cos(u\sin\psi) d\psi$$

$$J_2(u) = \frac{1}{\pi}\int_{\psi=0}^{\pi} \cos(u\sin\psi)\cos 2\psi d\psi \tag{3.18}$$

$$\vdots$$

$$J_n(u) = \frac{1}{\pi}\int_{\psi=0}^{\pi} \cos(u\sin\psi)\cos n\psi d\psi$$

Than, we can rewrite the y-component of A in the H-plane (3.17) as :

$$A_{yh} = \frac{\mu b I_o e^{-j\beta_o R_o}}{4R_o}\left[J_0(\sin\theta) - J_2(\sin\theta)\right] \tag{3.19}$$

Finally, the H-plane pattern can be easily obtained by substituting equation (3.19) into $E = -j\omega A$ (2.2) :

$$E_{yh} = \frac{-j\omega\mu b I_o e^{-j\beta_o R_o}}{4R_o}\left[J_0(\sin\theta) - J_2(\sin\theta)\right] \tag{3.20}$$

3.4 Radiation Patterns with the Ground Plane Factor

The second metal covered substrate is used as a reflector at a fixed distance behind the loop antenna. If we assume that the reflector plane is big enough and the metal cover may be approximated as a perfect conductor, the behavior of the reflector may be explained by using "image theory"[34].

Using this theory, the reflector plane may be removed by placing a virtual image current source S^- at a double distance 2d from the real current source S^+, as shown in Fig. 3.7. Note that the image current source is in the opposite direction of the real current source. If the real source S^+ and the image source S^- generate the radiation fields E^+ and E^-, respectively, the total field E should be the summation of the fields E^+ and E^-.

It is commonly assumed that the observation point P is located in the far-field region. In this region, we may ignore the amplitude difference of S^+ and S^- , but we have to take the phase difference into account:

$$E_y^- = -E_y^+ e^{-j\beta_o 2d\cos\theta} \tag{3.21}$$

In the right side of above equation, the first term with a minus sign shows that the directions of the image current source is opposite to that of the real current source. The second term shows the delay of the E^- to the E^+. For the H-plane pattern, we can write the total field E:

$$\begin{aligned} E_{yh} &= E_{yh}^+ + E_{yh}^- \\ &= E_{yh}^+ \left(1 - e^{-2j\beta_o d\cos\theta}\right) \\ &= E_o\left[J_o(\sin\theta) - J_2(\sin\theta)\right]\left(1 - e^{-2j\beta_o\cos\theta}\right) \end{aligned} \tag{3.22}$$

Similarly, we can obtain the E-plane pattern as:

$$\begin{aligned} E_{ye} &= E_{ye}^+ + E_{ye}^- \\ &= E_{ye}^+ \left(1 - e^{-2j\beta_o d\cos\theta}\right) \\ &= E_o\left[J_o(\sin\theta) + J_2(\sin\theta)\right]\left(1 - e^{-2j\beta_o\cos\theta}\right) \end{aligned} \tag{3.23}$$

In equations (3.22) and (3.23), E_o is the maximum value that the field intensity E can be reached, and E_o is determined by:

$$E_o = \frac{-j\omega\mu b I_o e^{-j\beta_o R_o}}{4R_o} \tag{3.24}$$

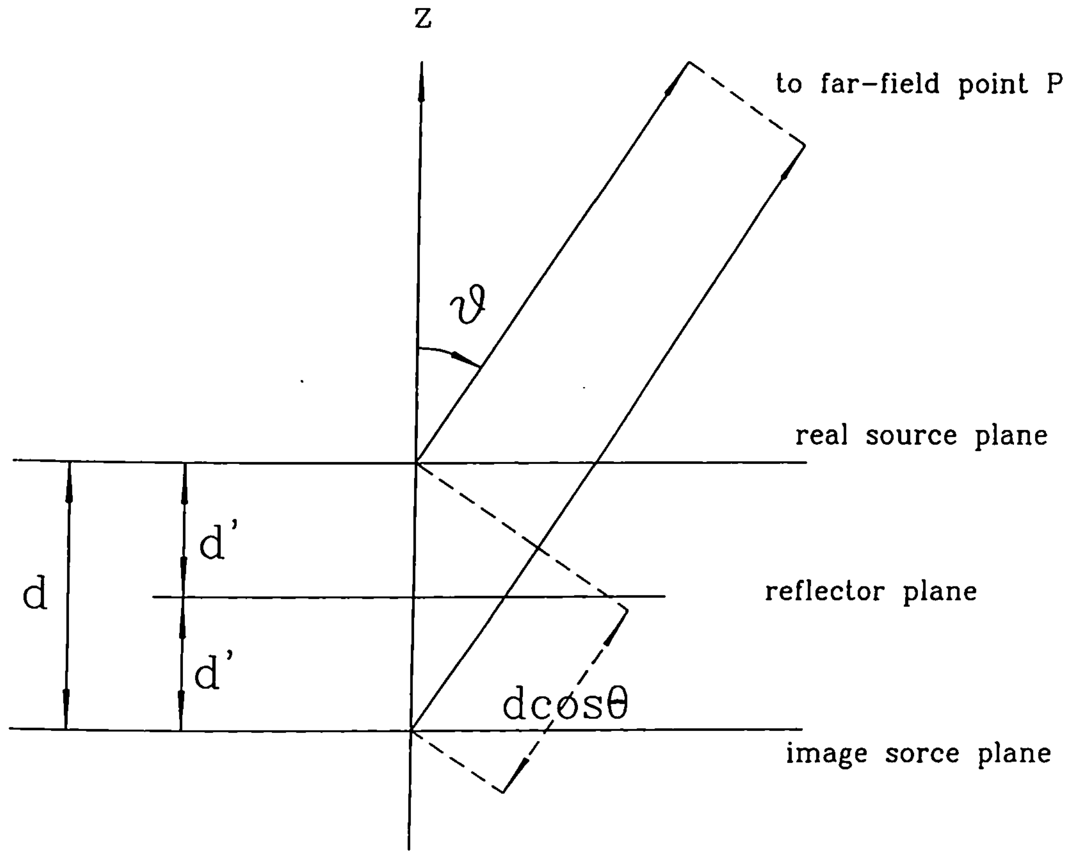

Fig. 3.7 *The reflector plane and the equivalent image source*

3.5 Radiation Patterns of Linear and Planar Arrays

As a mater of fact, equations (3.22) and (3.23) can be written in a more general form so that they cover both case of single radiating element and that of antenna arrays. By multiplying these two equations, (3.22) and (3.23), and the array factors (discussed in section 2.5) together, it follows that the general expressions of the radiation patterns are:

$$
\begin{aligned}
E_{yh} &= E_o\left[J_o(\sin\theta) - J_2(\sin\theta)\right]\left(1 - e^{-2j\beta_o\cos\theta}\right)AF \\
E_{ye} &= E_o\left[J_o(\sin\theta) + J_2(\sin\theta)\right]\left(1 - e^{-2j\beta_o\cos\theta}\right)AF
\end{aligned}
\tag{3.25}
$$

where, for single radiating element, AF=1; for linear arrays, AF is given in equation (2.24); and for planar arrays, AF is given by equation (2.25).

The far-field calculations using the equations in (3.25) shall be discussed with measured results of the microstrip loop antennas and arrays in next chapter.

Chapter 4

Antenna Design, Measurement and Simulations

4.1 Configurations of the Microstrip Loop Antenna

The microstrip loop antenna consists of two dielectric substrate plates which are placed parallel to each other with a spacing d. The first plate works as a radiator. The second plate is used both as a reflector and a ground plane.

In Fig. 4.1 is the first plate which is plotted as three separated layers to show the radiator configurations clearly. The radiating element is a ring patch

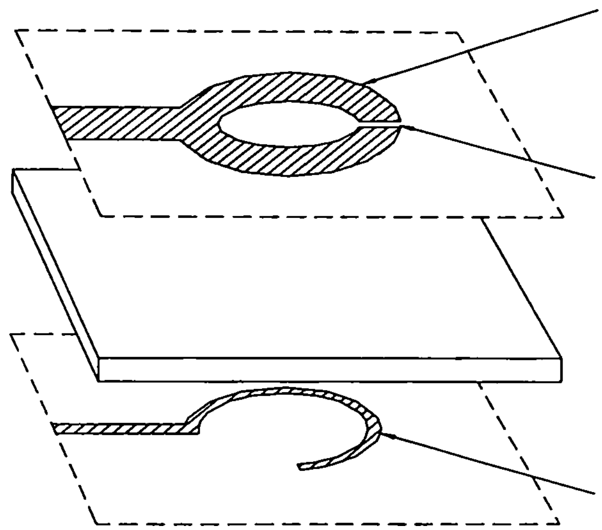

Fig. 4.1 *Configuration of microstrip Loop antenna (the first substrate plate)*

printed on the top surface of the first substrate. The median circumference of the ring is approximately one-wavelength (λ_g). Final design dimension of the circumference has to be determined experimentally. On the other side of the first plate is the feed line. Because the width of the feed line is much smaller than that of the ring, the structure of the ring-substrate-feedline may be considered as a microstrip circuit. There is a notch cut on the ring, providing an electromagnetic coupling between the radiating element and the feed line. The feed line is located on the under side of the radiating structure. It follows the structure of the ring patch, and extends beyond the coupling notch for a distance of a quarter wavelength. By adjusting the length of the extended portion of the feed line, the operational center frequency of the antenna can be adjusted until it equals to the desired frequency. Using this design, the following two advantages are obtained:

1. A compact structure. The radiating element of the microstrip loop antenna is fed by microstrip line. They are printed on the same dielectric board but on different sides. Electromagnetic energy is coupled via the notch cut on the ring patch. In this way, the radiator is constructed using only one dielectric board. In the SSFIP design, the radiating element and the feed line are printed individually on two dielectric boards, and these two boards are separated by a layer of foam. Both designs apply the similar techniques: microstrip feed line and slot coupling, but the microstrip loop antenna uses less material and assembling procedure is much easier. In addition, the geometrical size of the microstrip loop antenna is smaller than that of a SSFIP antenna. As we just mentioned, the median circumference of the ring is about one-wavelength, while the outside length of the rectangular patch is close to two-wavelengths.

2. The facility of building arrays. In the previous discussion about the current distribution in chapter 3, we knew that the current on a resonant loop can be represented as a sine function, and the current reaches its maximum value at the points of $\varphi=0$ and $\varphi=\pi$. According to the equations (2.16) and (2.18), we also note that near the point diametrically opposite to the notch, the electrical potential remains close to zero. Hence, we may connect two radiating elements and their feedlines at these points on the individual elements without changing

the antenna's operation. This simple fact gives the microstrip loop antenna a favorable feature: the structure can be easily expanded to build arrays for many potential applications.

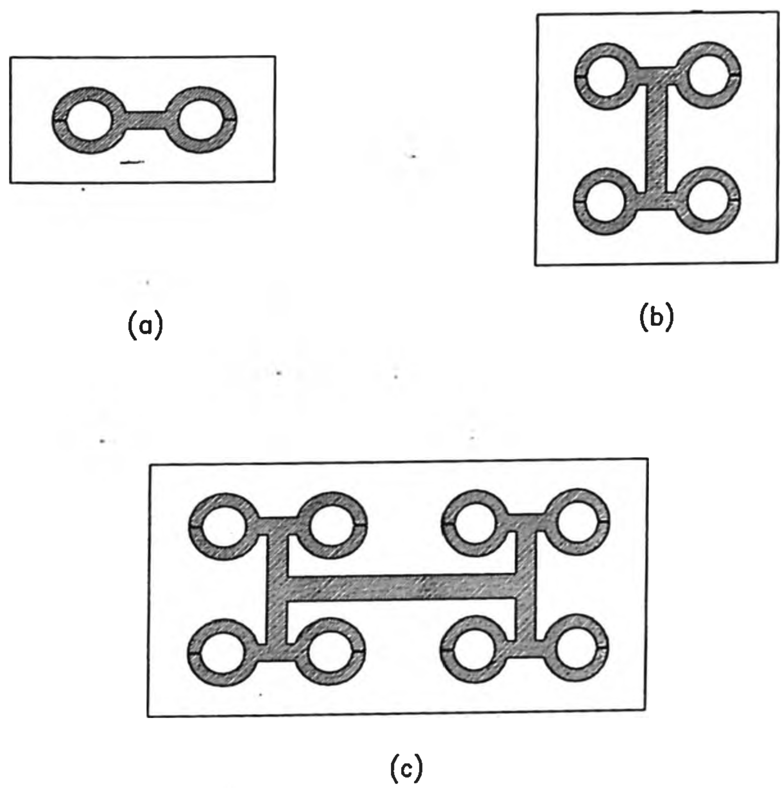

Fig. 4.2 *(a) 2-element array,* *(b) 4-element array,* *(c) 8-element array*

Fig. 4.2 gives some examples of arrays built in this way: 2-elements, 4-elements and 8-elements. As can be seen, the connections between two adjacent elements or two sub-arrays are straight lines. Obviously, this makes it easier to design the feed network of arrays which have a number of radiating elements. The measured and simulated results of these arrays shall be shown in a later section of this chapter.

The final part of the antenna topology is a metal covered substrate located at a fixed distance behind the antenna's radiating plate. This is used as a reflector to enhance the energy radiated in the forward direction. In addition, the second plate shields the antenna from interference arriving from the rear of the antenna, and is therefore called a ground plane. The performance of many antennas tends to be disturbed in practical situations because of the objects placed nearby. With the advent of wireless communications and microcells, more and more antennas will have to be installed within urban areas and even directly on the walls of buildings. Microstrip loop antennas are shielded by the presence of the ground plane, so whatever is located in the back of them does not significantly affect their operation.

4.2 Measured Performance I : The Dual-ring Antenna

To demonstrate the performance of the microstrip loop antennas, let us first look at the experimental results of a dual-ring antenna. The antenna consists of two symmetrical radiating elements, so it may also be viewed as a 2-element sub-array. Fig. 4.3. shows the antenna's configurations. By using the described design procedure, the antenna is constructed to operate at the frequency range of a CT2 personal communications system (PCS).

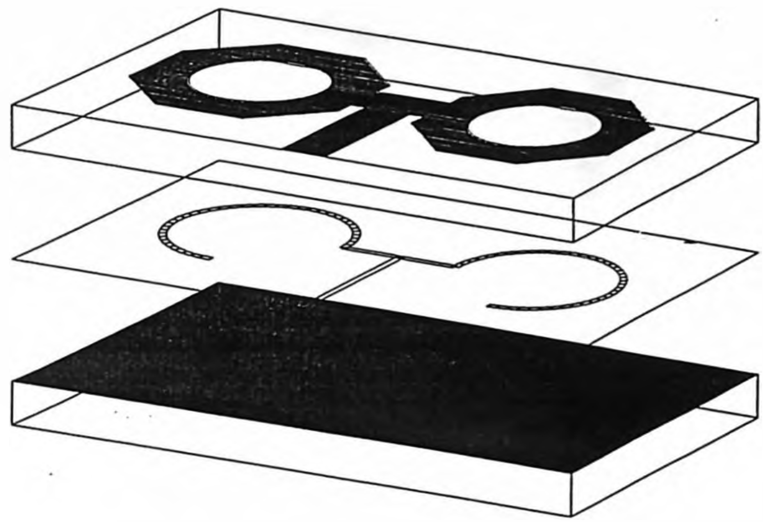

Fig. 4.3 *The dual-ring microstrip antenna*

The radiating elements are printed on a 1.57 mm thick FR4 glass epoxy substrate which is called printed-circuit board (PC board). Typically, FR4 PC board material is used only for low-frequency electronics circuits due to the fact that the dielectric-loss of FR4 increases as the microwave frequency is increased. However, the price of FR4 is typically much lower than the price of PC board material used at higher microwave frequencies. For wireless industry, it is clearly more favorable to build high performance antennas with low cost materials. The experimental results demonstrate that the dual-ring antenna indeed offers comparable performance to other microstrip antennas, but the difficulty of manufacturing and cost are much lower.

Fig. 4.4 shows the radiation patterns in the E-plane of the antenna, where the solid line represents the measured result. We observe a maximum gain of

11.2 dBi at 930 MHz frequency. The E-plane beam width is 71° , which is a little smaller than the width of the half-wavelength dipole antenna (78°).

In Fig. 4.5 are the H-plane patterns. Because there are two radiating elements arranged in the H-field direction, the H-plane beam is compressed by the effect of the array factor (section 3.5). The measured beam width in the H-plane is 46.1°. The highest level of the sidelobes and the backlobe is 18 dB lower than the value of the mainlobe.

From the return loss plot in Fig. 4.6, we can see that the dual-ring antenna has an operational frequency range from 846 to 1038 MH. This corresponds to a 20% bandwidth (i.e. the range over which a -10 dB less return loss is achieved). The experimental results show that the antenna's gain remains at an acceptable level as the working frequency is varied within this frequency bandwidth. For instance, the gain measured at 960 MHz remains is 10.8 dBi. When the frequency is shifted towards the lower edge of the band, the gain falls off slowly and the value measured at 920 MHz is 10.0 dBi.

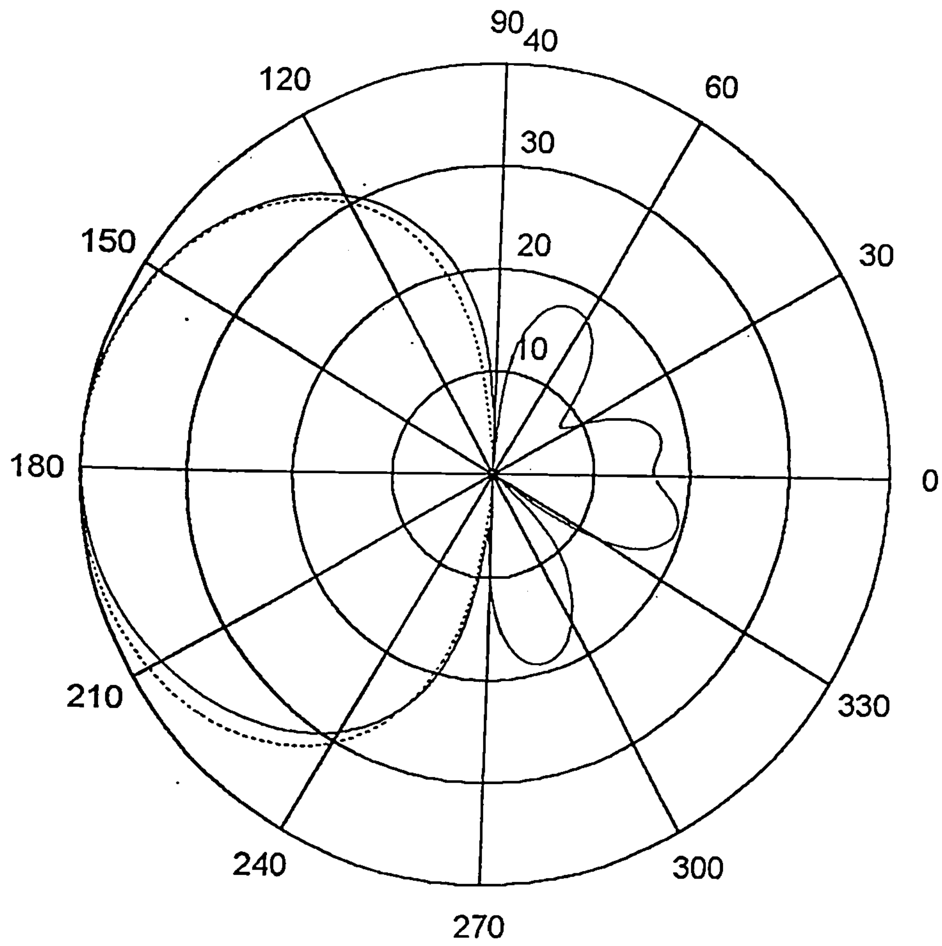

Fig. 4.4 *E-plane pattern of the dual-ring microstrip antenna*

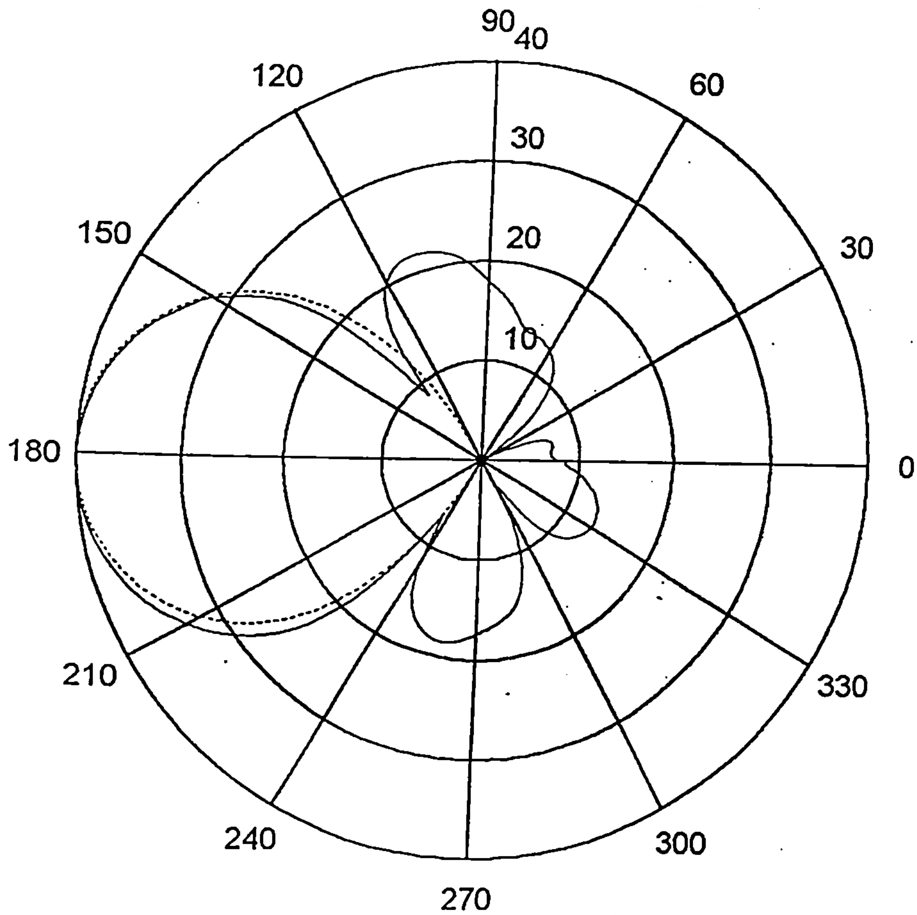

Fig. 4.5 *H-plane pattern of the dual-ring microstrip antenna*

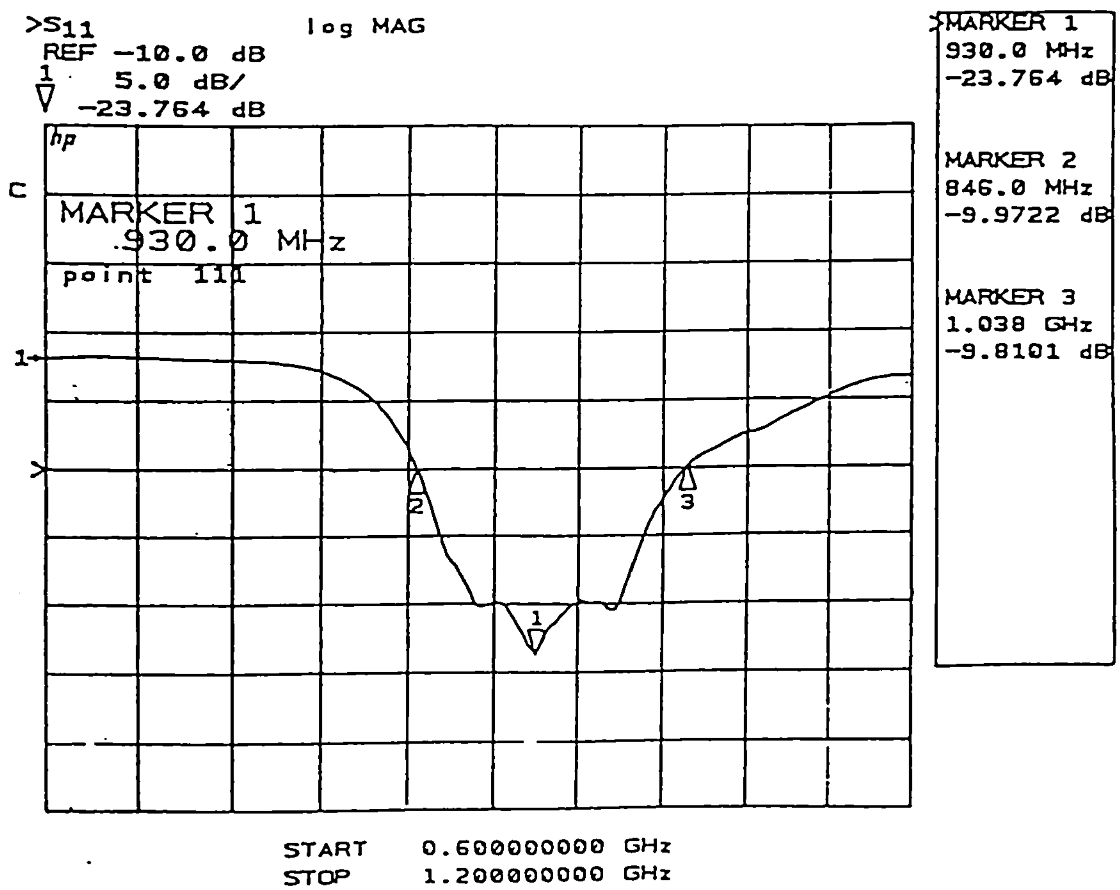

Fig. 4.6 *Return loss of the dual-ring microstrip antenna, BW=20%*

Table 4.1 gives the major radiation properties and antenna parameters of the dual-ring antenna and a single SSFIP antenna. As can be seen, the microstrip loop antenna offers improved performance by using a simpler structure and lower cost materials.

Table. 4.1 The performance and major antenna parameters of the dual-ring and a single SSFIP antenna

	working range(Hz)	gain (dBi)	BW (%)	cross-polar.(dB)	ε_r	layers
Loop	920~960M	10~11.2	20		4	2 substrates
SSFIP*	9.15~10.4G	8.2~8.8	13.2	-20~-25	2.33	3 substrates & 2 foams

* The SSFIP data is from reference [2].

4.3 Measured Performance II : Antenna Arrays

The antenna experiments were extended to the measurement of performance of 4-element and 8-element antenna arrays in two different operational frequency bands. Table 2 presents the results of these measurements. The frequency bandwidth observed during the experimental process is usually between 20-30%. The gain is about 13 dBi for the 4-element array and about 15 dBi for the 8-

element array. The increment of antenna gain is 1dB lower than the ideal 3dB value when the array size is doubled. One of the major reasons for the smaller than expected increment is the higher dielectric-loss of the PC board. Therefore, it is expected that higher gain will be realized if lower dielectric loss materials are used.

Table. 4.2 The performance of the microstrip loop arrays

elements	f_o (Hz)	gain (dB)	BW (%)	Crosspolar. (dB)	Sidelobe (dB)
4	915 M	13.2	22	-24	-13
8	915 M	15.2	21.7	-30	-9
4	2 G	11.4-13.0	29.3-36.8	-14	-17
8	2 G	15.2	30		-16

The feed network is a critical element in an array design. The design of an optimal network requires an intimate knowledge of power dividers and impedance matching of transmission lines [34] [36]. The results of our measurement show that the existing formulas for calculating impedance, based only on the width of the microstrip line, can only be used to make a preliminary design of the microstrip loop antenna. Changes and adjustments are necessary, and the feedline dimensions must be determined experimentally. The reasons for the discrepancies between existing design formula and actual performance are as follows:

- As was mentioned before, the microstrip loop antenna is only an approximate microstrip circuit;
- Since the ground plane is located near the antenna, it has an effect both on the performance of the antenna and on that of the feedlines;
- In addition to the difficulty of determining impedance of the feed lines, it is also difficult to obtain the load impedance both theoretically and experimentally (in this study, the load is the loop radiator). In traditional impedance matching techniques, such as the stub-tuning or the quarter-wave transformer, the load impedance has to be a known.

Although there is no suitable theoretical model which can be used to accurately calculate the antenna feed network, it is possible to match the radiating element to the feed structure. The formulas are used to derive an approximate match, and the final match is obtained experimentally. Experiments demonstrate that a short open-ended stub is the most effective way obtaining wideband impedance matching. Fig. 4.7 shows the return loss of a 4-element array, in which the feed network were adjusted experimentally. It is seen that a remarkable 36.8% bandwidth is achieved.

The experimental results also indicates that the performance of the microstrip loop antenna is not very sensitive to variations in the dimensions of the antenna element, as well as the feed network.

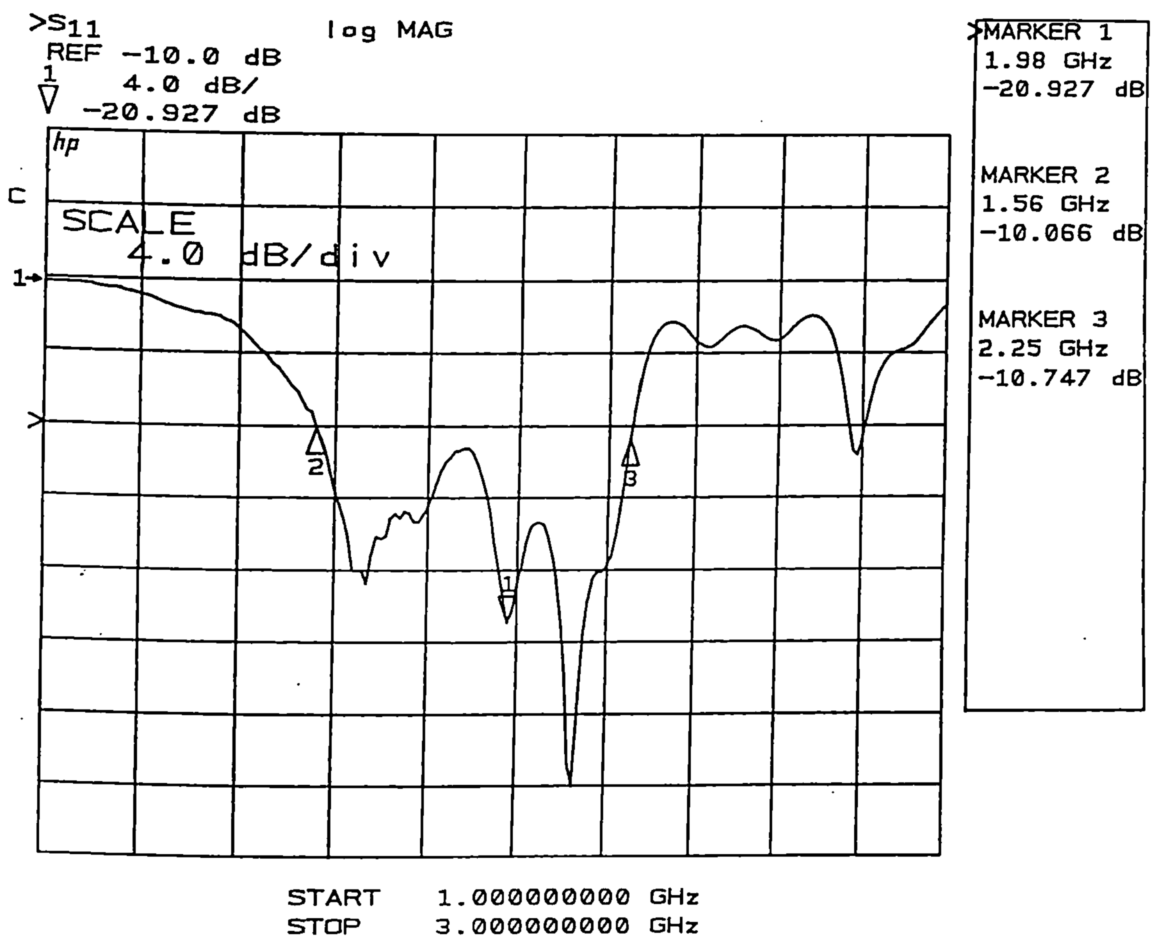

Fig. 4.7 *the return loss of a 4-element array with experimentally modified feed networks: a 36.8% bandwidth is achieved.*

In other words, once the parameters have been determined, the antenna has a high tolerance towards parameter variations which may be caused by material nonuniformity, by a small misalignment of the layers, or by changed dimensions that occur during the design and the assembling process. This is also a favorable feature especially in the production of large quantities of antennas.

In Table 4.2, it should be noted that the 8-element array, when working at 915 MHz, has a relatively high sidelobe level. The sidelobe is only -9 dB to the main lobe. The measured radiation pattern of the array is shown by the dotted line in Fig. 4.8. For most antenna applications, high sidelobes are undesirable because the signal received via the sidelobes can be of sufficient amplitude to interfere with the main beam signal.

The feed network used in this array incorporates four T-junction power splitters. These provide for an equal distribution of power over the eight elements of the array.

To reduce the sidelobe level, we can substitute these equal power splitters with unequal power dividers, in which way higher power is delivered to the elements located in the central region of the array and less power to the elements at the outer extremities of the array. In our investigations, the ratio of power division is chosen between 1.5:1 and 2:1, and a 6 dB improvement is observed. The solid line in Fig. 4.8 is the radiated pattern from an array driven by the unequal power division feed network. The sidelobe level is reduced from -9 dB to -15 dB.

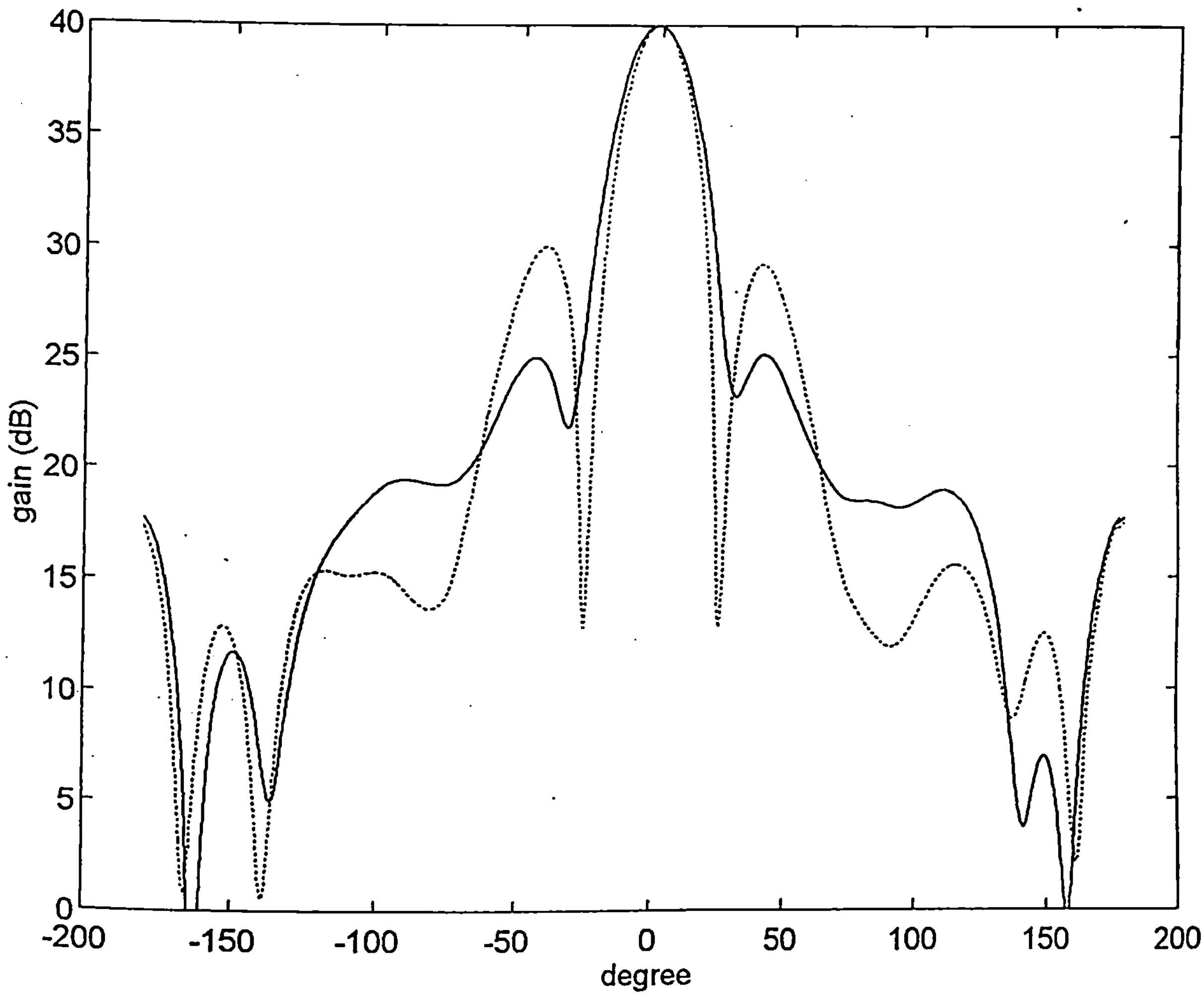

Fig. 4.8 *H-plane patterns of the 8-element array*

Dotted: equal-split feed; solid: unequal-split feed

4.4 Radiation Pattern Modeling

In our previous discussion about the radiation model of the loop antenna, we derived the formulas that can be used to calculate the E-plane and H-plane patterns. The formulas are also applicable to the case of linear or planar arrays, where we use the corresponding array factors discussed in Chapter 2.

For the dual-ring antenna, the calculated patterns (shown as the dotted lines) are plotted together with the measured patterns (the solid lines) in Figs. 4.4 and 4.5. As can be seen, the calculated results are very close to the measured patterns in the main-lobe region. In the side-lobe and back-lobe regions, difference appears between the calculation and measurements. This is because the model is developed under the assumption that the ground plane is an infinitely large and perfect conducting plane, but this is not the case in practice.

For the cases of 4-element and 8-element arrays, simulations based on this model, also show very good results, as shown in Figs. 4.9 and 4.10 where the dotted lines are the calculated patterns and the solid lines are the measured patterns.

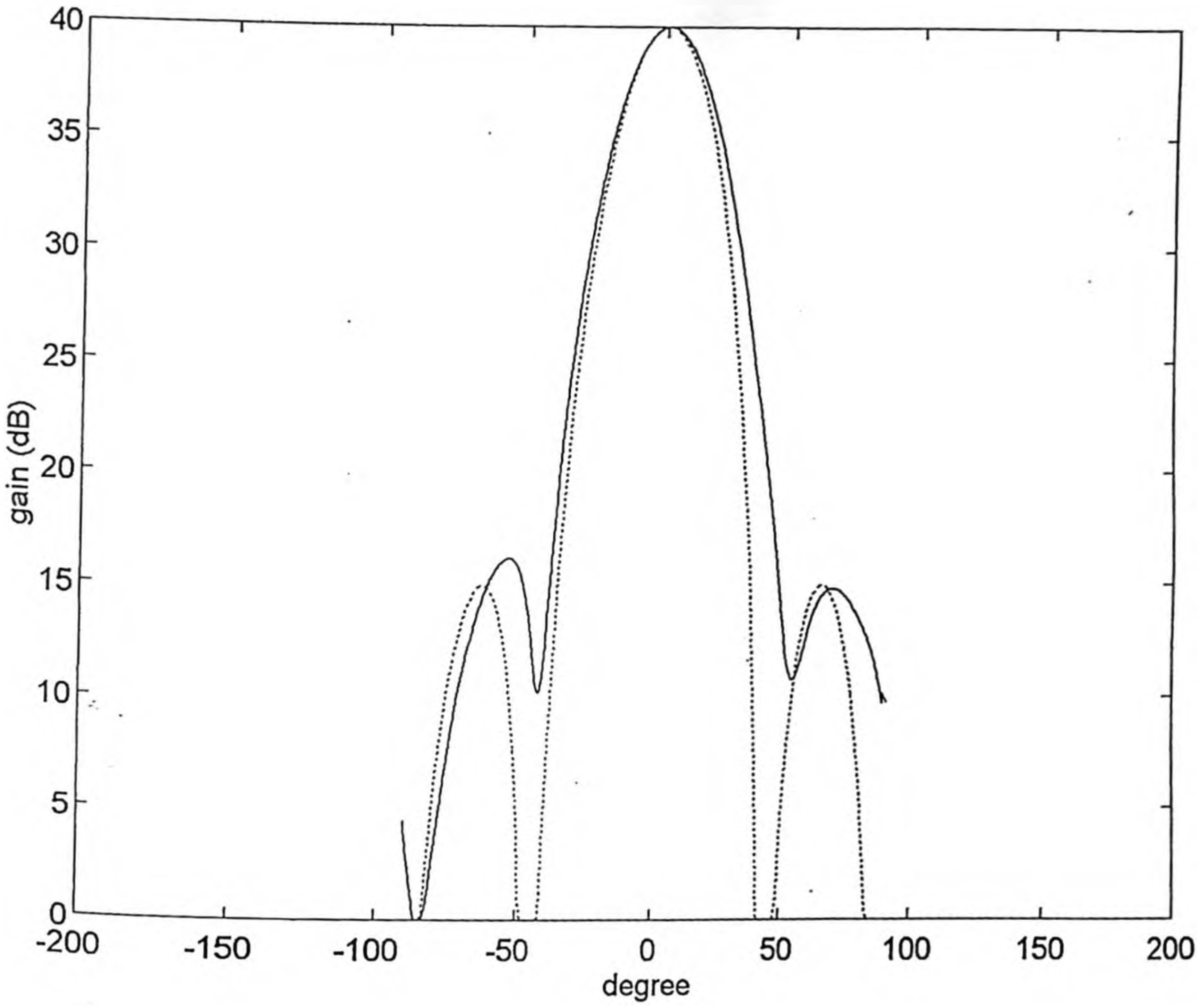

Fig. 4.9 *H-plane patterns of the 4-element array (2 GHz)*

Dotted: simulation; solid: measured pattern

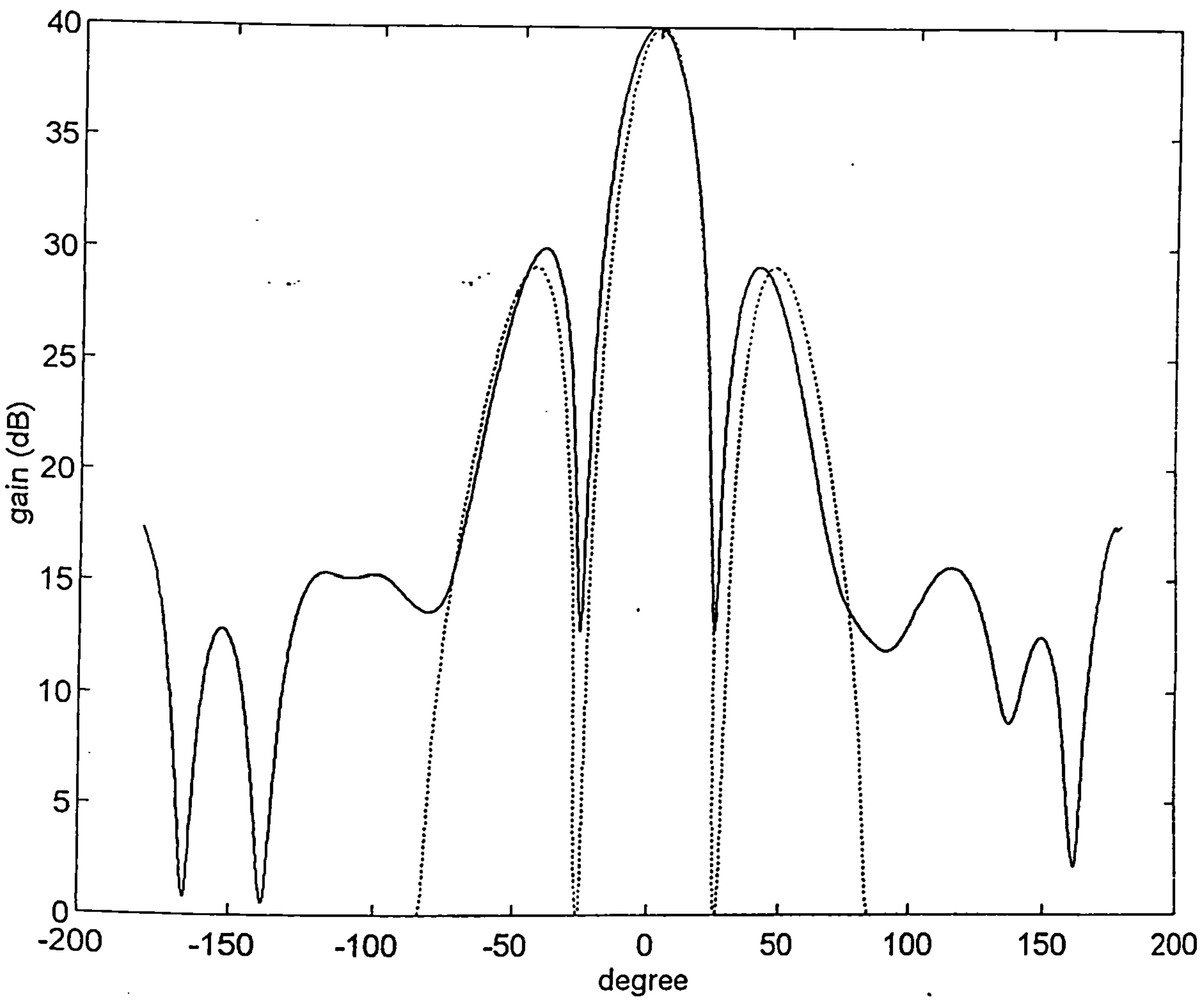

Fig. 4.10 *H-plane patterns of the 8-element array (915 MHz)*

Dotted: simulation; *solid: measured pattern*

Chapter 5

Conclusions and Discussions

For a long time, microstrip antennas were characterized by a narrow frequency band and low radiation efficiency. Many researchers and users tended to consider these properties as inherent to the microstrip structure itself.

Attempts have been made to increase the bandwidth of microstrip antennas by using complex geometry in which several modes interact. Other approaches use one or several additional radiating elements, which have sizes that are slightly different from that of the main radiating element. These elements are also called "parasitic elements" [37][38]. However, the most effective way to achieve broadband operation is to increase the substrate thickness and to reduce the permittivity [2].

In recent years, significant developments have been made with SSFIP antennas. Developers of these antennas have made significant improvements to the bandwidth of microstrip antennas by using multilayer structures, thick substrates, materials with low permittivity, and parasitic radiating elements. There are also several papers in the literature which describe use of array elements which are dual-polarized or circular-polarized.

In comparison with SSFIP antennas, the microstrip loop antennas in this study offer improved performance with much less complexity and lower production cost. Extensive experiments were carried out using of single-radiating-elements and antenna arrays in different operational frequency bands. The results of these investigations can be summed as follows:

1. The loop shape of the microstrip antenna offers better bandwidth performance than the SSFIP antenna. The measured bandwidth of a single-loop element is found to be between 10-24%, while the bandwidth of a single-SSFIP is not likely to exceed 14-15% [2]. For microstrip loop array antennas, the observed bandwidth is between 20-37%.

2. Because fewer layers are used in the microstrip loop antenna, its design and manufacturing procedures are simpler than that of the SSFIP

antenna. Furthermore, the loop antenna offers comparable gain properties by using inexpensive substrate materials (see table I and table II). It is reasonable to believe that the microstrip loop antenna provides a favorable alternative for low-cost consumer applications.

3. Microstrip feedlines and electromagnetic coupling are used in the antenna design, therefore, there is no soldering required between the feed structure and the radiators. The antenna's layout also makes it easy to group many radiating elements to form linear or planar arrays, so the antenna has many potential applications.

A model for loop antenna radiation is also made by using a nonuniform current approach. This method gives a very clear physical explanation of the antenna operation. The derived field formulas can be conveniently used to calculate far-field patterns because of their simple forms. This is particularly true for the case of antenna arrays. For optimum design, the formulas can be used to determine the appropriate spacing for the best patterns of the antenna.

References

1. K. Fujimoto and J. R. James, Mobile Antenna Systems Handbook, Artech House, Inc. 1994

2. Jean-François Zürcher and Fred E. Gardiol, Broadband Patch Antennas, Artech House, Inc. 1995

3. J. R. James, P. S. Hall and C. Wood, Microstrip Antenna Theory and Design, IEE, London: Peter Peregrinus, 1981

4. D. H. Schaubert, F. G. Farrar, A. Sindoris, and S. T. Hayes, "Microstrip antennas with frequency agility and polarization diversity", IEEE Trans. Antennas Propag., vol. AP-29, no. 1, pp. 118-123, January 1981

5. W. F. Richards and Y. T. Lo, "Theoretical and experimental investigation of a microstrip radiator with multiple lumped linear loads", Electromagnetics, vol. 3, no. 3-4, pp. 371-385, Duly-December 1983

6. W. F. Richards, Y. T. Lo, and D. D. Harrison, "An improved theory of microstrip antennas with applications", IEEE Trans. Antennas Propag., vol. AP-29, no. 1, pp. 38-46, January 1981

7. W. F. Richards and S. A. Long, "Impedance control of microstrip antennas utilizing reactive loading", Proc. Intl. Telemetering Conf., pp. 285-290, Las Vegas, 1986

8. W. F. Richards and S. A. Long, "Adaptive pattern control of a reactively loaded dual-mode microstrip antenna", Proc. Intl. Telemetering Conf., pp. 291-296, Las Vegas, 1986

9. R. J. Mailloux, J. McIlvenna, and N. Kernweis, "Microstrip array technology", IEEE Trans. Antennas Propag., vol. AP-29, no. 1, pp. 25-38, January 1981

10. G. Dubost, Flat Radiating Dipoles and Applications to Arrays, Chichester, Research Studies Press, 1981

11. D. M. Pozar, "Analysis and Design Considerations for Printed Phased-Array Antennas", in J. R. James and P. S. Hall, Eds., Handbook of Microstrip Antennas, Vol. 1, Chap. 12, London, Peter Peregrinus, 1989

12. G. A. Deschamps, "Microstrip microwave antennas", presented at the 3rd USAF Symp. on Antennas, 1953

13. R. E. Munson, "Single slot cavity antennas assembly", U. S. Patent No. 3713162, January 23, 1973

14. Keith R. Carver and James W. Mink, "Microstrip antenna technology", IEEE Trans. Antennas Propag., vol. AP-29, no. 1, pp. 2-24, January 1981

15. R. E. Munson, "Conformal microstrip antennas and microstrip phased arrays", IEEE Trans. Antennas Propag., vol. AP-22, no. 1, pp. 74–78, January 1974

16. A. G. Derneryd, "A theoretical investigation of the rectangular microstrip antenna element", IEEE Trans. Antennas Propag., vol. AP-26, no. 4, pp. 532-535, July 1978

17. Y. T. Lo, D. Solomon, and W. F. Richards, "Theory and experiment on microstrip antennas", IEEE Trans. Antennas Propag., vol. AP-27, no. 2, pp. 137-145, March 1979

18. J.-F. Zürcher and F. É. Gardiol, "The SSFIP, a Global Concept for High Performance Broadband Planar Antennas", IEE Electronics Letters, Vol. 24, p1433-1435, 1988

19. F. É. Gardiol and J.-F. Zürcher, "Broadband Patch Antennas - a SSFIP Update", IEEE Antennas and Propagation Society International Symposium, Vol. 1, pp. 2-5, 1996

20. M. Edimo, P. Rigolant, and C. Terret, "Wideband Dual Polarized Aperture-Coupled Stacked Patch Antenna Array Operating in C-Band", IEE Electronics Letters, Vol. 30, pp. 1196-1198, 1994

21. E. Aloni, and R. Kastner, "Analysis of a Dual Circularity Polarized Microstrip Antenna Fed by Crossed Slots", IEEE Trans. Antennas Propag., vol. AP-42, pp. 1053-1058, 1994

22. A. Taflove and K. R. Umashankar, "The Finite-Difference Time-Domain Method for Numerical Modeling of Electromagnetic Wave Interactions", Electromagnetics, Vol. 10, pp. 105-126, 1990

23. J. R. Mosig, "Integral Equation Techniques for Three-Dimensional Microstrip Structures", in R. Stone, Ed. Review of Radio Science 1990-1992. London, Oxford University Press, pp. 127-152, 1993

24. Jianming Yang, John Litva, Chen Wu and Tony Tam. "Practical Microstrip Dual-ring Antenna", IEE Electronics Letters, Vol. 32, No. 6, pp. 511-512, Mar. 1996

25. Jianming Yang, Chen Wu and John Litva, "Microstrip Ring Antennas for PCS Application", IEEE Antennas and Propagation Society International Symposium, Vol. 3, pp. 1594-1597, 1996

26. Warren L. Stutzman and Gary A. Thiele, Antenna Theory and Design, John Wiley & Sons, New York, 1981

27. H. Hertz, Electric Waves, Macmillan and Co. Ltd., London, 1893

28. R. W. P. King and G. S. Smith, Antennas in Matter: Fundamentals, Theory, and Applications, The M.I.T. Press, Cambridge, Mass., 1981

29. John D. Kraus, Antennas, McGraw-Hill Book Company, Inc., New York, 1950

30. Donald Foster, "Loop Antennas with Uniform Current", Proc. I. R. E., Vol. 32, pp. 603-607, 1944

31. Ronold W. P. King and Sheila Prasad, Fundamental Electromagnetic Theory and Applications, Prentice-Hall, Inc., Englewood Cliffs, N. J. , 1986

32. R. E. Collin and F. J. Zucker, Antenna Theory, part 1, McGraw-Hill Book Company, Inc., New York, 1969

33. Glenn S. Smith, "Chapter 5: Loop Antennas", in Richard C. Johnson, Ed., Antenna Engineering Handbook, 3th-edition, pp. 5-1~5-16, McGraw-Hill, Inc., New York, 1993

34. David M. Pozar, Microwave Engineering, Addison-Wesley Publishing Company, New York, 1990

35. Edward A. Wolff, Antenna Analysis, Artech House Inc., Norwood, 1988

36. J. R. James and P. S. Hall, Microstrip Antenna Theory and Design, Peter Peregrinus Ltd., London, 1981

37. C. K. Aanandan and K. G. Nair, "Compact broadband Microstrip Antenna", IEE Electronics Letters, Vol. 22, pp. 1064-1065, 1986

38. H. K. Smith and P. E. Mayes, "Stacking Resonators to Increase the Bandwidth of Low Profile Antennas", IEEE Trans. Antennas Propag., vol. 35, pp. 1473-1476, 1987

39. C. Wu, K.-L. Wu, Z.-Q. Bi and J. Litva, "Accurate characterization of planar printed antennas using finite -difference time-domain method", IEEE Trans. Antennas Propag., 40 (5), pp526-534, May 1992

40. P. F. Combes, J. Graffuil and J-F. Sautereau, Microwave Components, Devices and Active Circuits, Translated from the French by W. J. Duffin, John Wiley & Sons Inc., Chichester, 1987

Appendix

Guidelines for deriving the dimensions of a loop antenna design

Step 1: The fundamental discussions for the loop antenna

In a previous discussion regarding radiation from the microstrip loop antenna which was given in Chapters 2 and 3, we noted that the radiation is due to a sinusoidal current distributed on the loop surface. We may also say that the antenna is a resonant antenna since it works in its first order resonant mode:

$$I(\phi) = I_o \cos\phi, \qquad 0 \le \phi \le 2\pi \qquad \text{A-1}$$

This condition requires that the antenna dimension have to be one wavelength, i.e.:

$$2\pi r = \lambda_g \qquad \text{A-2}$$

where r is the radius of the loop, and λ_g is the wavelength of the wave in the dielectric substrate. Clearly, it is of primary importance when designing a loop antenna to determine the dimension r, because it defines the antenna's operational frequency.

Step 2: Determination of the equivalent relative permittivity ε_e

For a microstrip line, λ_g is depended on the equivalent relative permittivity ε_e which can be determined by following formulas [40]:

$$\lambda_g = \frac{\lambda_o}{\sqrt{\varepsilon_e}} \qquad \text{A-3}$$

In this equation, λ_o is the wavelength in free space, and the ε_e takes a value in a range of :

$$1 < \varepsilon_e < \varepsilon_r \qquad \text{A-4}$$

where, ε_r is the relative permittivity of the dielectric substrate. To calculate ε_e of a microstrip line, we may use the following equations provided by Gardiol (1981) [40]:

(i) for the strips with a ratio of width to thickness w/h>1,

$$\varepsilon_e = \frac{1}{2}(\varepsilon_r + 1) + \frac{1}{2}(\varepsilon_r - 1)\left(1 + 12\frac{h}{w}\right)^{-\frac{1}{2}} \qquad \text{A-5}$$

(ii) for the strips with w/h⩽1,

$$\varepsilon_e = \frac{1}{2}(\varepsilon_r + 1) + \frac{1}{2}(\varepsilon_r - 1)\left[\left(1 + 12\frac{h}{w}\right)^{-\frac{1}{2}} + 0.04\left(1 - \frac{w}{h}\right)^2\right] \qquad \text{A-6}$$

where h is the thickness of the substrate and w is the width of the strip line. More detailed discussions about using these formulas for different situations are available in above marked reference.

It should be noted that these formulas are not an exact fit to our antenna configurations. Although at best they are an approximation, we still want to use them to do the calculation. The main discrepancies between our antenna topology and the first-order equations are : (i) our antenna topology is not strictly a microstrip topology (this was mentioned in Chapter 4) ; and (ii) the radiating structure is located in proximity to a reflecting plane. Obviously, these tow factors are not included in these formulas, and we will encounter errors when using these formulas to design our antenna.

Unfortunately, no formulas exist at the present time for calculating the effective dielectric constant for our antenna structure. However, the calculation errors can easily be corrected by using experimentally derived data.

Step 3: Use of experimental data for correcting the calculated results

First, we build a test antenna using the calculated ε_e and λ_g, and test the performance by measuring the return loss and the radiation patterns. Generally speaking, there will be a frequency shift $\Delta\lambda_g$ between the desired frequency λ_g and the tested one λ'_g:

$$\Delta\lambda_g = \lambda_g - \lambda'_g \qquad \text{A-7}$$

From equation A-3, we have:

$$\Delta\varepsilon_e = -2\sqrt{\varepsilon_e}^{\,3}\frac{\Delta\lambda_g}{\lambda_o} \qquad \text{A-8}$$

where $\Delta\lambda_g$ is the test data obtained from measurement, and $\Delta\varepsilon_e$ is the correction item which we are going to add to the original ε_e given by A-5 or A-6 . Correspondingly, the λ_g given by A-3 is modified as a new one by:

$$\lambda_g = \frac{\lambda_o}{\sqrt{\varepsilon_e + \Delta\varepsilon_e}} \qquad \text{A-9}$$

Then, we can replace the old λ_g in A-2 with the new one in A-9 to determine the radius of the loop.

Repeat this correction procedure several times if necessary until the tested frequency is consistent with the desired one.